Core cross-linked polymeric micelles based on polypept(o)ides: from secondary structure formation of polypeptides to functional cross-linking strategies for polymeric micelles

Bauer, T.A.

4

Tuning the Cross-Linking Density of Polymeric Micelles and its Implications on Particle Stability in Human Blood Plasma

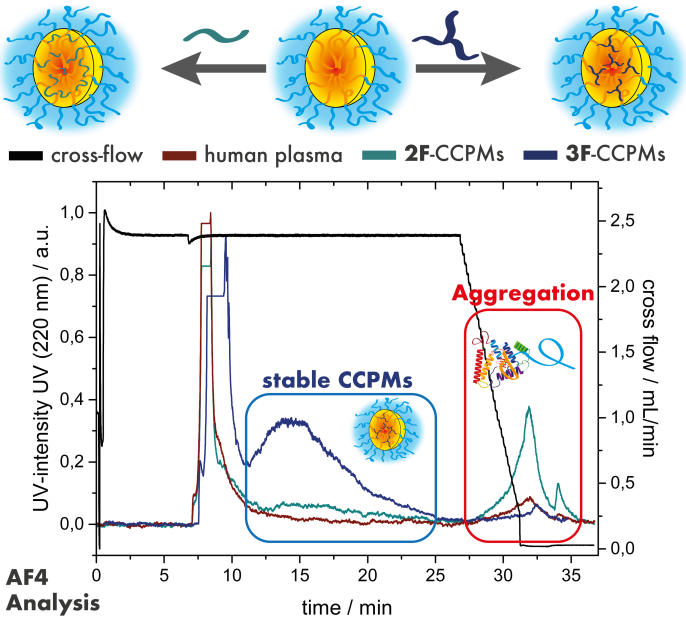

to be submitted to Biomacromolecules.

Tuning the Cross-Linking Density of Polymeric Micelles and its Implications on Particle Stability in Human Blood Plasma

Tobias A. Bauer[a, b], Irina Alberg[b], Lydia A. Zengerling[b], Heyang Zhang[a], Pol Besenius[b], Kaloian Koynov[c], Bram Slütter[a], Rudolf Zentel[b], Matthias Barz[a, b,*]

[a] Leiden Academic Centre for Drug Research (LACDR), Leiden University, Einsteinweg 55, 2333 CC Leiden, The Netherlands

[b] Department of Chemistry, Johannes Gutenberg University Mainz, Duesbergweg 10-14, 55128 Mainz, Germany

[c] Max Planck Institute for Polymer Research, Ackermannweg 10, 55128 Mainz, Germany

to be submitted to Biomacromolecules.

Abstract

Core cross-linked polymeric micelles (CCPMs) are designed to improve the biodistribution of hydrophobic drugs aiming for an improved therapeutic profile. Compared to non-stabilized structures, cross-linking reduces the protein corona formation and prolongs the circulation half-life of the carrier. In this study, we provide details on how to tune the particle stability by using bi- or trifunctional cross-linkers and varying the length of the cross-linkable polymer block. For disulfide bond cross-linked polymeric micelles, amphiphilic thiol-reactive polypept(o)ides of polysarcosine-*block*-poly(*S*-ethylsulfonyl-L-cysteine) (pSar-*b*-pCys(SO_2Et)) are employed as the building block with pCys(SO_2Et) chain lengths of X_n = 17 or 30. For cross-linking, derivatives of dihydrolipoic acid and a sarcosine/cysteine pentapeptide are employed. Analysis by asymmetrical flow field-flow fraction (AF4) after incubation with human blood plasma clearly shows aggregate formation for non-cross-linked nanoparticles, yet surprisingly for CCPMs cross-linked with dihydrolipoic acid at X_n = 17. Increasing the cross-linking density leads to more stable nanoparticles in AF4, whereby a structure-activity relationship can be detected. Conversely, no differences are detectable by fluorescence correlation spectroscopy in human blood plasma or *in vivo* after intravenous administration to male C57BL/6 mice. In conclusion, our study provides a first insight on how to adjust CCPM stability for *in vivo* application as drug delivery systems.

Keywords

polymeric micelles · polypept(o)ides · AF4 · cross-linking · nanomedicine

Introduction

Nanomedicine offers the potential to alter the biodistribution of active pharmaceutical ingredients (API) and may provide additional selectivity to the potent substances. For hydrophobic drugs, polymeric micelles are the preferred carrier system.[1,2] Within the core-shell architecture, the drug mainly resides in the inner hydrophobic core, and the hydrophilic corona provides solubility and shielding.[2,3] Following Nanomedicine 2.0 for drug targeting beyond replacing solubilizers, carrier and cargo need to be stabilized to prevent premature carrier disintegration and drug release immediately after administration.[4–6] The primary connection between amphiphilic copolymer and self-assembled polymeric micelle thus needs to be disrupted, by either non-covalent kinetic trapping (e.g., by π-π interactions, hydrogen bonding) or dynamic covalent bonds, i.e., by cross-linking.[6–9] Depending on the cargo, polymeric micelles can be cross-linked by individual strategies. For transition metal-complexes such as platin or ruthenium-based APIs, the drug itself can act as a cross-linker allowing for drug release upon ligand exchange.[10–13] Furthermore, click chemistry, amide bond formation, and free radical cross-linking are frequently employed to provide stability to polymeric micelles and allow, among others, for the conjugation of taxane and anthracycline (pro-) drugs.[14–17] Despite the early developed Genexol-PM and Nanoxel, non-cross-linked polymeric micelles (e.g., Bind-014, NK105) could not further demonstrate their superiority in clinical testing.[18,19] As a result, core cross-linked polymeric micelles (CCPMs) are considered the second generation of polymeric micelles and evolved to advanced stages of clinical testing. Currently, CPC634 containing conjugated docetaxel is examined for the treatment of ovarian cancer in clinical phase II, and NC-6004 comprising cisplatin is assessed in phase III for pancreatic cancer therapy.[19,20]

Due to the inherent potential for stable cross-linking yet reversible drug release after cellular uptake, disulfide bonds have attracted significant interest.[17,21] While disulfide cross-linked micelles can be readily formed from thiol-containing copolymers by oxidation with oxygen in a rather unspecific manner, the reactive *S*-alkylsulfonyl protecting group introduced by Schäfer *et al.* offers chemoselective disulfide bond formation.[22–25] Applied to cysteine or homocysteine the reactive group tolerates nucleophilic amine-initiated *N*-carboxyanhydride (NCA) polymerization and grants access to thiol-reactive polypeptides.[26–28] The combination of polypeptides with polysarcosine (pSar) in so-called polypept(o)ides is a straightforward approach leading to copolymers entirely based on endogenous

amino acids.[29,30] Polysarcosine, poly(*N*-methyl glycine), is an exclusive hydrogen bond acceptor characterized by random coil structure in aqueous solution matching all requirements stated by the Whitesides rules.[31,32] The hydrophilic pSar is thus considered the most promising alternative to poly(ethylene glycol) (PEG) for biomedical applications showing an improved safety profile such as a reduced induction of cytokine release.[33–37]

Beyond the intended chemical design of a nanoparticle, protein corona formation has been reported to determine the fate of many nanocarriers upon administration into the bloodstream.[38–41] Unambiguous signs of the protein corona were detected for nanoparticles with sharp and hydrophobic surfaces (e.g., polystyrene, silica nanoparticles) affecting the biological profile.[39,42–44] For nanoparticles with a smoothly decreasing radial density profile, such as CCPMs shielded with a dense corona of either PEG, pSar, or poly(*N*-(2-hydroxypropyl)methacrylamide), conversely, the absence of protein corona formation was observed.[40] Hereby, analysis by asymmetrical flow field-flow fractionation (AF4) was used to separate nanoparticles and nanoparticle/protein complexes after incubation with human blood plasma followed by high-resolution mass spectrometry.[40] Separation by AF4 relies solely on the diffusion of the analyte in the separation channel, whereby a parabolic flow profile is combined with an orthogonal cross-flow toward a semipermeable membrane.[45,46] Depending on Brownian motion, smaller structures elute earlier than larger assemblies or aggregates, while interactions with the static phase are minimized.[45,46] The interaction of blood plasma proteins with amphiphilic copolymers originating from insufficiently stabilized nanocarriers can thus be detected by AF4.[16,45,46] Non-cross-linked micelles are in constant equilibrium between unimers and micelles. Therefore, the situation is quite complex as the interaction of plasma proteins with amphiphilic polymers leads to defects in the hydrophilic shell. The defect sites are then prone to unspecific interaction, and the released free polymer may assemble to polymer/protein aggregates.[16,44,47]

The outlined strategies for core cross-linking could already demonstrate the potential to improve the carrier stability and control drug release *in vivo*.[48] Nevertheless, up to now, little attention was paid to the influence of the cross-linking itself, namely, how do cross-linker functionality and the length of the cross-linkable block contribute on the overall particle stability and in vivo performance. We now investigate the effect of the core size and length, and the valency of the cross-linker on the stability of polymeric micelles prepared from

thiol-reactive polysarcosine-*block*-poly(*S*-ethylsulfonyl-L-cysteine) using AF4 and fluorescence correlation spectroscopy (FCS) in human blood plasma for evaluation. We further correlate these results to the circulation half-life and biodistribution analysis after intravenous administration of CCPMs to C57BL/6 mice with the view toward defining parameters for CCPM stability.

Results and Discussion

Polymeric micelles are frequently applied as carrier systems for hydrophobic drugs, whereby cross-linking has already been demonstrated to improve the circulation time of the nanocarrier.[2,6,48] The aim of this study was to investigate whether the cross-linker or the length of the cross-linkable block has a relevant influence on the particle stability in human blood plasma. Therefore, functional cross-linkers were synthesized, and core cross-linked polymeric micelles prepared from polypept(o)ides building up on our previous reports.[49–51] As shown in Scheme 1, the polymeric micelles (PMs) were formed by self-assembly of thiol-reactive amphiphilic block copolymers of pSar-*b*-pCys(SO_2Et). In a second step, the *S*-ethylsulfonyl group was converted by chemoselective disulfide bond formation with the thiol-reagents. Thereby, the length of the cross-linkable pCys(SO_2Et) block was varied from X_n = 17 to 30 ($PM_{17/30}$), whereas the length of the pSar block was kept constant at X_n = 200 to provide sufficient steric shielding.

Since cross-linking itself is not sufficient to prevent premature drug release,[52] hydrazide-modified cross-linkers that grant stimuli-responsive drug conjugation were designed.[53] Even after the CCPM synthesis, these groups allow for coupling of ketone-bearing (pro-) drugs such as doxorubicine, epirubicine, or conjugates of taxanes with levulinic acid.[54] In detail, CCPMs were prepared from bifunctional dihydrolipoic acid hydrazide (2F-$CL_{17/30}$) and the trifunctional cysteine-sarcosine pentapeptide (3F-$CL_{17/30}$). The trifunctional pentapeptide was synthesized by solid-phase peptide synthesis, and the hydrazide linker was introduced *via* coupling with *N*-*tert*-butyloxycarbonyl-succinic acid monohydrazide in a consecutive step (Scheme S3). The alternating structure of sarcosine and cysteine was selected to provide solubility since pure polycysteine forms insoluble anti-parallel ß-sheets that complicate the application.[55] As a control, non-cross-linked micelles were prepared by quenching the *S*-ethylsulfonyl group with monofunctional methyl 3-mercaptopropionate ($NCL_{17/30}$). The reagent was selected based on similar molecular weight and hydrophobicity compared to the

S-ethylsulfonyl group, while considering the odor nuisance and toxicity of small molecule thiol compounds such as ethanethiol.

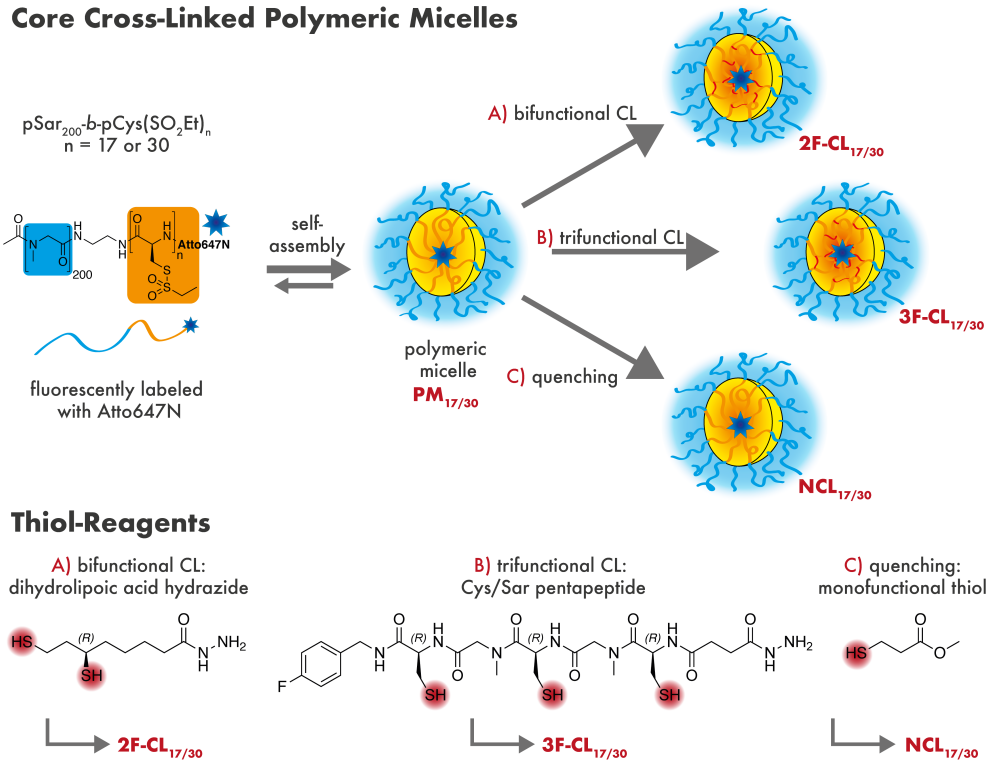

Scheme 1. Preparation of core cross-linked polymeric micelles from pSar-*b*-pCys(SO_2Et)$_n$ with n = 17 or 30 and thiol-reagents of varying functionality.

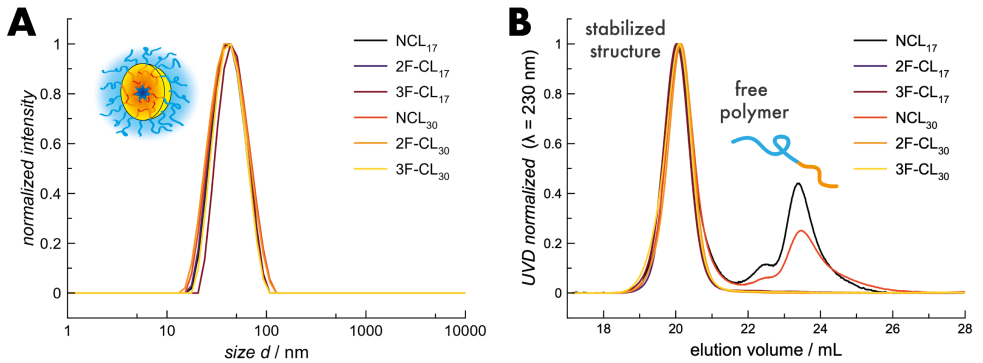

Figure 1. Nanoparticle characterization by DLS (**A**) and HFIP-GPC (**B**).

When analyzed by dynamic light scattering (DLS), all particles showed similar hydrodynamic diameters around 40 nm with narrow dispersities of 0.06 to 0.1 (Figure 1). The cross-linking or quenching reaction did thus not affect the overall size distribution.[50] Furthermore, for the cross-linked particles (2F-CL and 3F-CL) only stabilized structures but no unimers could be detected by HFIP-GPC after purification. Vice versa, significant amounts of free polymer could be detected for non-cross-linked particles. Despite the strong anti-parallel ß-sheet formation of pCys which accounts for the stabilized structures correlating with the chain length (free polymer content: NCL_{30} < NCL_{17}), a certain degree of cross-linking originating from disulfide-exchange reactions cannot be excluded.[56] Nevertheless, successful conversion of the *S*-ethylsulfonyl group could be verified by ^{1}H NMR, referring to the assigned methoxy group (Figure S2).

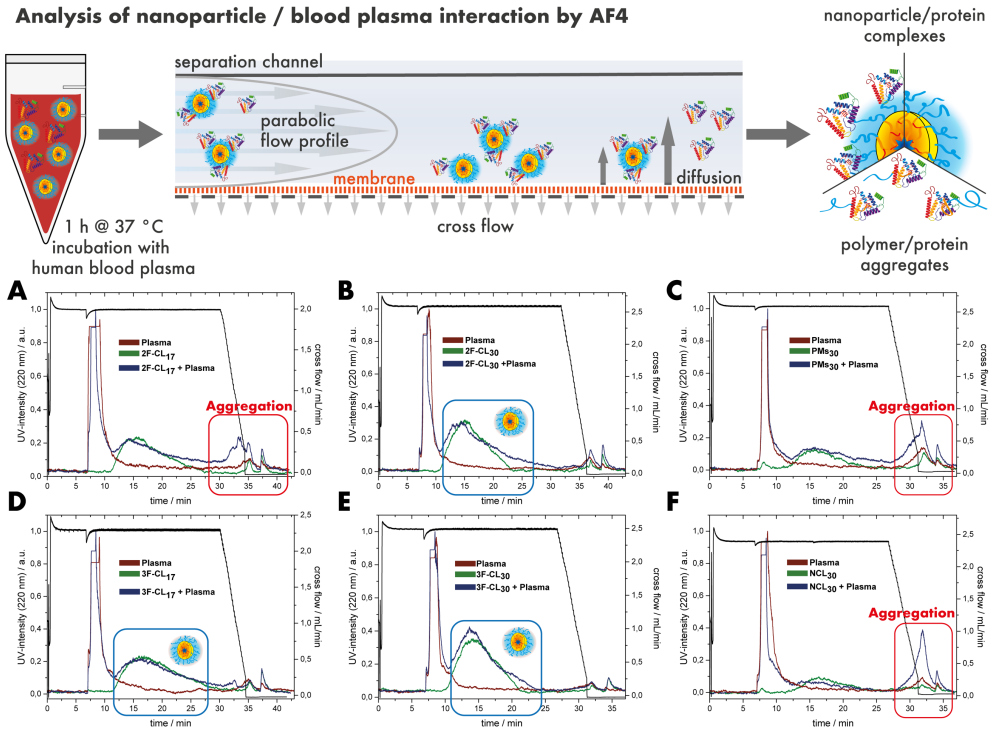

Figure 2. Analysis of CCPMs by AF4 after incubation with human blood plasma. The results of the AF4 analysis as detected by UV absorbance (λ = 220 nm): CCPMs after incubation in PBS (green) or human blood plasma (blue), and plasma controls (red). The following particles have been used: $2F\text{-}CL_{17}$ (**A**), $2F\text{-}CL_{30}$ (**B**), PMs_{30} (**C**), $3F\text{-}CL_{17}$ (**D**), $3F\text{-}CL_{30}$ (**E**), NCL_{30} (**F**).

In the following, the polypept(o)ide-based nanoparticles were analyzed by AF4 and FCS in human blood plasma. The procedure of the AF4 analysis is shown in Figure 2. As illustrated, the samples were incubated in either PBS or human blood plasma for 1 h at 37 °C. Hereby, a regenerated cellulose membrane (pore size 10 kDa) and a cross flow of up to 2.5 mL/min was applied. The isolated nanoparticle-protein complexes or polymer/protein aggregates were then detected based on UV-absorbance and light scattering (LS) intensity. For well stabilized structures, identical elution profiles are expected regardless of the incubation in human plasma.[16,40]

For all samples incubated in PBS (green color), a distinct particle peak could be identified by the UV-detector at elution times of 10-20 min (Figure 2A-F). After incubation in human blood plasma, however, aggregate formation was detected when the cross flow was again reduced to 0 mL/min and a rinse-peak at 30-40 min became visible, as in the case of 2F-CL_{17} (Figure 2A). Since these nanoparticles were considered stable previously, showing no free polymer in HFIP-GPC, no aggregation when analyzed by multi-angle DLS after incubation in human blood plasma as well as decent circulation time in zebrafish embryos and mice,[49,57] this set the motivation for the detailed study. In fact, when the cross-linking density was enhanced by increasing the number of available net-points, the rinse peak could be reduced significantly following the sequence 2F-CL_{17} < 2F-CL_{30} < 3F-CL_{17} < 3F-CL_{30}. Changing the cross-linker functionality from 2 to 3 appears slightly more effective for stabilization than (almost) doubling the cross-linkable polymer block, which reflects the gel-point theory for polymerization of multifunctional monomers (Carothers equation). In addition, for the CL_{30} species, the particle peak became slightly broader after incubation with blood plasma, which could indicate an increased protein corona formation.[40] On the other hand, for PM_{30} and NCL_{30} the particle peak almost entirely vanished after incubation in blood plasma leading to a strongly elevated rinse peak (Figure 2C and 2F). Beyond detection by UV-absorbance, light scattering is even more sensitive to large structures providing extra resolution to AF4. As shown in Figure 3, the insufficiently stabilized samples 2F-CL_{17}, PM_{30}, and NCL_{30} show almost no particle peak but only a large fraction of aggregates after incubation with human blood plasma. Furthermore, the rinse peak practically disappeared for 3F-CL_{30} with intermediate intensities for 2F-CL_{30} > 3F-CL_{17} supporting the findings from the UV-detection.

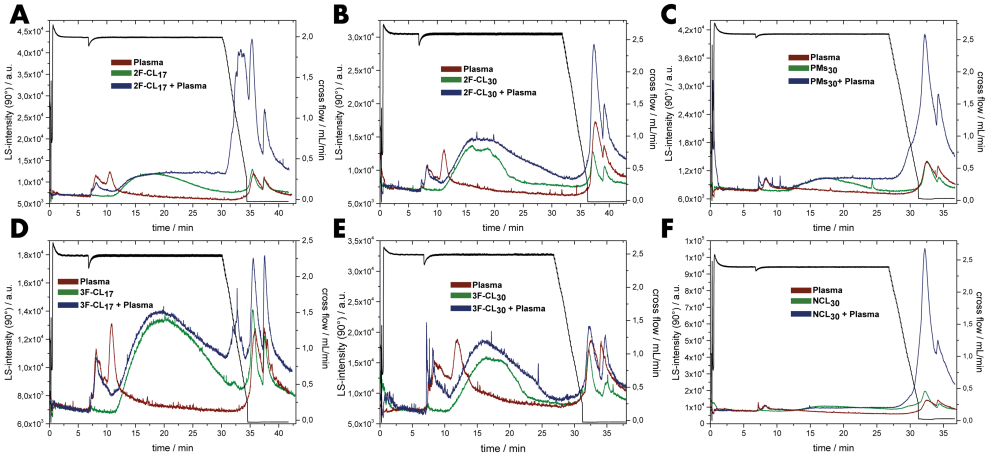

Figure 3. Results of the AF4 analysis as detected by light scattering (scattering angle: 90°): CCPMs after incubation in PBS (green) or human blood plasma (blue), and plasma controls (red). The following particles have been used: 2F-CL_{17} (**A**), 2F-CL_{30} (**B**), PMs_{30} (**C**), 3F-CL_{17} (**D**), 3F-CL_{30} (**E**), NCL_{30} (**F**).

Opposing on the trend of the particle stability revealed by AF4, analysis by FCS in human blood plasma did not detect any differences among the samples (Figure 4). In aqueous solution, hydrodynamic radii from 19 to 21 nm were detected for all particles, which is in good agreement with the results from DLS. In addition, no remaining free dye (Atto647N) could be detected. However, the exact same radii were calculated after incubation with human blood plasma regardless of cross-linking (2F-$CL_{17/30}$ and 3F-$CL_{17/30}$) or quenching ($NCL_{17/30}$). FCS is a precise method to determine the size of colloids, nanoparticles or proteins.[58] Moreover, following the procedure established by Negwer *et al.*, FCS can even be applied directly in human blood.[59] FCS relies on the diffusion of the fluorescent probe through the small confocal observation volume. The diffusion coefficient can be derived from the autocorrelation function translating to the hydrodynamic radius *via* the Stokes-Einstein relation. Alterations in the radius or the quality of the fit indicate interaction, aggregation, or protein corona formation with high sensitivity.[59,60] The unchanged radii of 19 to 21 nm thus indicate stable particles in both conditions.

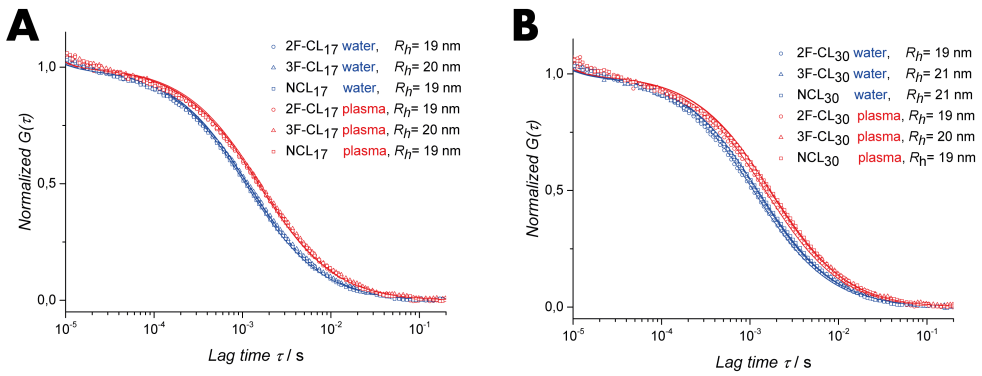

Figure 4. Results of the FCS analysis in water (blue) and plasma (red): The normalized autocorrelation functions *G(τ)* are given for nanoparticles prepared from pSar-*b*-pCys(SO_2Et)$_{17}$ (**A**) or pSar-*b*-pCys(SO_2Et)$_{30}$ (**B**) and monofunctional, bifunctional or trifunctional cross-linkers. The hydrodynamic radii were derived *via* the Stokes-Einstein relation.

To relate the contradictory results of the two screening techniques to the *in vivo* situation, the cross-linked (2F-CL$_{30}$ and 3F-CL$_{30}$) and not-cross-linked (NCL$_{30}$) nanoparticles were investigated for their circulation time and biodistribution. As displayed in Figure 5A, the nanoparticles were administered to C57BL/6 mice by intravenous injection, and blood samples were taken at the indicated time intervals and analyzed for nanoparticle-associated fluorescence. In addition, the tissue exposure was measured by *ex vivo* organ imaging after 72 h post injection. The results of the *in vivo* study are displayed in Figure 5, and all screening data are summarized in Table 1.

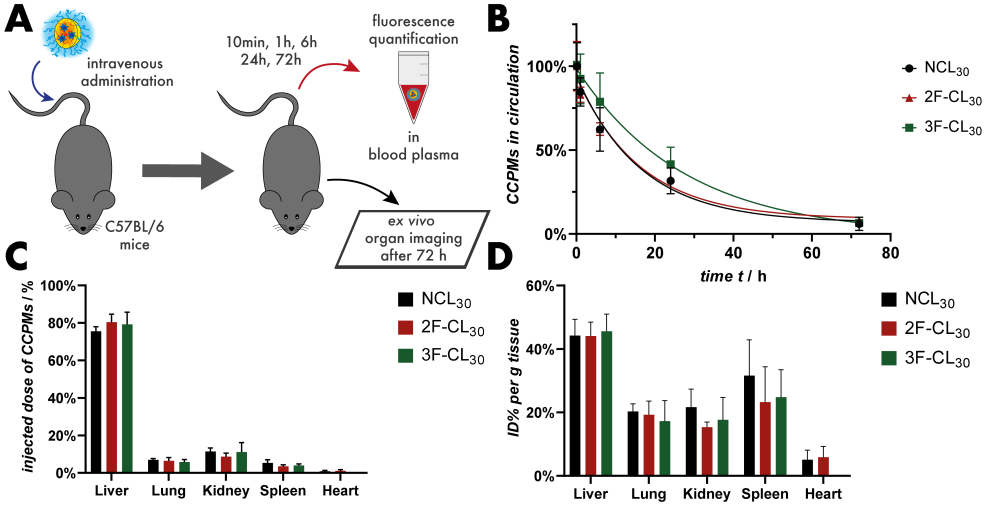

Figure 5. Evaluation of cross-linked and non-cross-linked polymeric micelles in C57BL/6 mice. Schematic illustration of the *in vivo* experiment (**A**). Nanoparticle circulation time analysis calculated from the nanoparticle fluorescence in blood plasma samples. Normalization to 10 min time point, fit model: mono-exponential decay (**B**). Nanoparticle biodistribution in liver, lungs, kidneys, spleen, and heart after 72 h post injection based on the total fluorescence intensity in *ex vivo* organ imaging (**C**). Nanoparticle biodistribution in liver, lungs, kidneys, spleen, and heart after 72 h post injection based on the fluorescence intensity relative to the organ weight in *ex vivo* organ imaging (**D**).

For all particle groups, circulation half-lives of 11.3 h - 19.1 h were detected. Interestingly, no clear trend could be derived among the treatment groups. Within the error of the mean ($N \geq 4$) and the calculated 95% confidence intervals (CI), no significances could be detected for any distinct time point or the circulation half-life. Nevertheless, compared to NCL_{30} and 2F-CL_{30}, 3F-CL_{30} showed a slightly decreased clearance as higher particle contents could be detected at 6 h ($p \leq 0.265$) and 24 h ($p \leq 0.261$) post-administration. For the accumulation of the nanoparticles in the liver, lung, kidney, spleen, and heart no significant differences could be detected among the treatment groups. In absolute numbers, approx. 80% of the total fluorescence intensity were detected in the liver. Relative to the tissue weight, approx. 40% and 30% can be detected in liver and spleen. Since the liver is the major organ for nanoparticle clearance, the predominant accumulation could aid to improve the toxicologic profile of drugs with high toxicity to the heart (doxorubicine) or the kidneys (cisplatin), while the long circulation time sets the basis for passive tumor targeting via the EPR effect.[19,61,62]

Table 1. Summary of the nanoparticle characterization and evaluation.

particle	D_h / nm[a]	*PDI*[a]	R_h / nm[b]	R_h / nm[c]	AF4-score[d]	$t_{1/2}$ / h[e]	*CI* ($t_{1/2}$) / h[e]
NCL_{17}	39	0.06	19	19	-	-	-
2F-CL_{17}	39	0.09	19	19	3	-	-
3F-CL_{17}	43	0.08	20	20	2	-	-
NCL_{30}	40	0.09	21	19	4	11.4	6.8 - 18.7
2F-CL_{30}	38	0.10	19	19	2	11.3	7.4 - 17.1
3F-CL_{30}	40	0.07	21	20	1	19.1	12.3 - 34.8

[a] DLS in PBS; [b] FCS in PBS; [c] FCS with human plasma; [d] AF4 with human plasma, qualitative score: 1: no interaction detectable, 2: slight rinse peak detectable, 3: large rinse peak detectable, 4: large rinse peak detectable and particle peak vanished; [e] intravenous administration in C57BL/6 mice, fluorescence detection from plasma samples, fit model: mono-exponential decay.

Taken together, we applied AF4 and FCS to determine the stability of disulfide cross-linked polymeric micelles in human blood plasma with the aim to derive structure-activity relationships predicting the *in vivo* fate. AF4 analysis revealed a very detailed image of the nanoparticle properties, clearly linking the number of cross-linkable groups to the tendency to form polymer/protein aggregates. Conversely, FCS analysis in human plasma did not indicate any aggregation or undesired interaction of nanoparticles and blood plasma components. In a similar manner, upon intravenous administration, no differences could be detected for the circulation half-life or biodistribution of cross-linked or non-cross-linked particles based on pSar-*b*-pCys(SO_2Et). However, the error bars of the circulation time analysis are relatively large, preventing narrow confidence intervals. Furthermore, the 10 min time point, which was used for normalization, may have been selected too late, since initial drop values are typically observed for structures without additional stabilization.[63,64] Of note, even for the NCL particles additional stabilization by antiparallel ß-sheets needs to be taken into account, as well as possible cross-linking by disulfide shuffling, as mentioned above.[51,55,56] Despite the clear improvement of the particle stability as recognized by AF4 upon increasing the cross-linker functionality and the length of the cross-linkable section, it remains challenging to derive the quantitative means. In particular, light scattering is very sensitive to large structures ($I \sim r^6$), potentially overrating a small fraction of the sample. On the other hand, both, FCS and the *in vivo* experiment only refer to the particle fluorescence, and thus a number weighted

result, in which a small species may simply be overlooked. Considering the careful development of a medicinal product, all signs of aggregation or interaction of the product with blood plasma components need to be taken very seriously, as they may affect the patient compliance and the patient's life. Our findings thus provide a valuable insight on nanoparticle stability in human plasma and detection thereof.

Conclusion

We have investigated core cross-linked polymeric micelles for their stability in human blood plasma by AF4 and FCS and correlated the results to the biodistribution and circulation half-life after intravenous administration in C57BL/6 mice. Based on thiol-reactive polypept(o)ides of $pSar_{200}$-*b*-$pCys(SO_2Et)$, the length of the cross-linkable $pCys(SO_2Et)$ block was chosen 17 or 30. The polymeric micelles were cross-linked by linkers with varied functionality. Bifunctional dihydrolipoic acid hydrazide and a trifunctional Cys/Sar pentapeptide were used to generate core cross-linked particles. Monofunctional methyl 3-mercapto propionate was applied to convert the reactive *S*-ethylsulfonyl group into a disulfide bond without intending any cross-linking. After incubation in human blood plasma, AF4 analysis revealed a clear connection between the nanoparticle stability and the number of net points or the cross-linker functionality. Clear signs of aggregation could be detected for non-cross-linked structures. Opposing on these results, FCS analysis in human blood plasma did not detect any signs of aggregation or protein corona formation for any sample. Moreover, a similar biodistribution and comparable circulation half-times of 11.3 - 19.1 h were found for all nanoparticles, indicating no significant differences. The observed variances may be attributed to the sensitivity and detection modes of the analytical techniques. For the optimal design of nanomedicines, our findings demonstrate how the stability of CCPMs can be adjusted most efficiently.

Experimental Section

Materials and Methods: All solvents and reagents were used as received as purchased from Sigma-Aldrich, unless stated otherwise. Fmoc-L-cysteine(Trt)-OH, Fmoc-sarcosine, and 2-chlorotrityl chloride-resin were obtained from Iris Biotech GmbH, HFIP and trifluoroethanol (TFE) were purchased from Fluorochem, 1-[Bis(dimethylamino)methylene]-1H-1,2,3-triazolo[4,5-b]-pyridinium 3-oxide hexafluorophosphate (HATU) was obtained from Carbolution,

deuterated solvents were obtained from Deutero GmbH, and (*R*)-lipoic and was bought from TCI Europe. Atto647N *N*-hydroxysuccinimide (NHS) was obtaind from Atto Tec GmbH. Tetrahydrofuran (THF) was dried over Na and was freshly distilled before use. *N*,*N*-Diisopropylethylamine (DIPEA) and *N*,*N*-triethylamine (NEt_3) were dried over sodium hydroxide, distilled, and stored at -20 °C until further use. *N*,*N*-Dimethylformamide (DMF) (99.8 %, extra dry over molecular sieve) was bought from Acros Organics and purified by freeze-pump-thaw cycles to remove dimethyl amine. MilliQ water was prepared by using a MILLI-Q Reference A+ System and used at a resistivity of 18.2 $M\Omega \cdot cm^{-1}$ and total organic carbon (TOC) content of ≤ 5 ppm.

Column chromatography: Qualitative thin layer chromatography (TLC) was performed on silica coated aluminum sheets (60 Å, F_{254}) with a fluorescence indicator from *Merck*. The detection of the analytes was performed with UV light (λ = 254 nm). Purification *via* size-exclusion chromatography (SEC) was performed using a Sephadex® LH-20 column with methanol or chloroform/methanol (1:1).

Gel Permeation Chromatography: For gel permeation chromatography (GPC), a Jasco GPC setup was used operating on a flow rate of 1.0 mL min^{-1} at 40°C. HFIP equipped with 3 $g \cdot L^{-1}$ of potassium trifluoroacetate was used as eluent and toluene as the internal standard. Three PFG columns (particle size 7 µm, porosity 100 Å, 300 Å, and 4000 Å) were used for separation (PSS Polymer Standards Service GmbH, Germany), and poly(methyl methacrylate) standards (PSS Polymer Standards Service GmbH, Germany) and pSar standards were used for calibration.[31] A UV detector (UV-4070, λ = 230 nm) was used for polymer detection and data were analyzed using PSS WinGPC.

Infrared Spectroscopy: Attenuated total reflectance Fourier transform infrared (ATR-FT-IR) spectroscopy was performed on a FT/IR-4600 spectrometer (Jasco Corporation) equipped with a Jasco ATR Pro ONE unit using Jasco spectra manager 2.15.18 for data evaluation

Nuclear Magnetic Resonance: The NMR spectra were recorded at room temperature on Avance II 400, Avance III 400, Avance I 500, or Avance III 600 spectrometers (Bruker). DOSY NMR spectra were recorded on the Bruker Avance I 500 using a bipolar pulse program (stebpgp1s) with d20 = 0.2 and p30 = 2750 µs for gradient amplitudes from 5 to 95%. Spectra were calibrated

using the solvent signals and the data were analyzed using MestReNova 14.1.2 (Mestrelab Research S.L.).

Single-Angle Dynamic Light Scattering: DLS measurements were performed on a Zetasizer Ultra (Malvern Panalytical Ltd.) equipped with a He-Ne laser (λ = 632.8 nm). The measurements were performed at 25 °C and at a detection angle of 173° using disposable half-micro polystyrene cuvettes (Carl Roth GmbH & Co. KG, Germany). The cumulant size, polydispersity index (PDI), and size distribution histograms (intensity weighted) were derived from the autocorrelation function using automated position seeking and attenuator selection at multiple scans, with fluorescence filter.

Polymer Synthesis: The polymers were prepared by ring-opening NCA polymerization in anhydrous DMF using flame-dried glassware and Schlenk conditions. Sarcosine-NCA and *S*-ethylsulfonyl-L-cysteine-NCA were synthesized as published previously.[22,30]

Polysarcosine: The pSar macroinitiator was synthesized according to our previous reports.[50,51]

Briefly, sarcosine-NCA (9.18 g; 79.8 mmol; 220 eq.) was transferred to a flame-dried Schlenk tube and dissolved in degassed absolute DMF (50 mL). Next, *N*-(*tert*-butoxycarbonyl)-1,2-diaminoethane (58.1 mg; 363 µmol; 1.0 eq.) was added as a stock solution in dry DMF (ß = 20 g·L^{-1}). The polymerization was stirred at 10 °C shielded from light until the monomer peaks had vanished in IR spectroscopy (9 days). Subsequently, the amine end-group was reacted with perfluorophenyl-4-azidobutanoate (215 mg; 725 µmol; 2.0 eq.) and DIPEA (308 µL; 1.81 mmol; 5.0 eq.). The reaction was stirred overnight. Next, acetic anhydride (346 µL; 3.63 mmol; 10 eq.) and DIPEA (1.23 mL; 7.25 mmol; 20 eq.) were added and the reaction was stirred for one day at room temperature. The polymer was precipitated in diethyl ether (500 mL), centrifuged (4500 rpm; 3 min; 4°C), and the pellet collected and was dried *in vacuo*. In the following, the Boc-group was cleaved. The crude polymer was transferred to a single-neck round-bottom flask and dissolved in water (25 mL). The solution was cooled to 0 °C and trifluoro acetic acid (25 mL) was added in one portion. The reaction mixture was stirred at 0 °C for 4 h. The solution was transferred into 3 dialysis bags (MWCO, 3.5 kDa) and dialyzed against water (2 medium changes), sodium hydrogen carbonate solution (8 medium changes), and water (8 medium changes). The polymer solution was filtered and lyophilized. Polysarcosine (P1) was obtained as

a colorless solid (4.04 g, 71%). Complete deprotection was verified by ^{1}H NMR (absence of the Boc-group signal at 1.37 ppm). The degree of polymerization was determined by HFIP GPC relative to pSar standards (*DP* = 200). ^{1}H NMR (500 MHz, DMSO-*d*$_6$): δ (ppm) 4.49 - 3.80 (m, 2nH, -CH$_2$), 3.03 - 2.66 (m, 3nH, -CH$_3$).

Polysarcosine-block-Poly(S-Ethylsulfonyl-L-Cysteine): The block copolypept(o)ides were synthesized following our previous reports.[50,51] The pSar macroinitiator (P1) (523 mg; 36.6 µmol; 1.0 eq.) was weighed into a flame dried Schlenk tube and the solid was dried by azeotropic distillation with toluene (2x). Next, pSar was dissolved in freshly degassed dry DMF (5.75 mL) and cooled to -10 °C. Then, *S*-ethylsulfonyl-L-cysteine NCA (438 mg; 1.83 mmol; 50 eq.) was added from a stock solution in dry DMF (β = 200 g·L^{-1}). The reaction was performed at an overall NCA concentration of β = 55 g·L^{-1}. The reaction progress was monitored by IR spectroscopy, and the reaction was stopped after 20 h, when a conversion of 38% was detected (correlating to DP 19). The polymer was precipitated in THF, and the suspension was centrifuged (4500 rpm; 5 min; 4 °C) and decanted. The procedure was repeated once with THF followed by diethyl ether for two times. The polymer was dried *in vacuo* yielding pSar$_{200}$-*b*-pCys(SO$_2$Et)$_{17}$ (P2) as a colorless solid (600 mg, 68%). For P3, pSar$_{200}$-*b*-pCys(SO$_2$Et)$_{30}$, the polymerization was performed at an overall NCA concentration of β = 100 g·L^{-1} and the reaction was stopped at 60% conversion. For dye labeling, the copolymer (P2, 142 mg; 8.1 µmol; 1.0 eq.) was dissolved in DMSO, Atto647N-*N*-hydroxysuccinimide (2.59 mg; 3.08 µmol; 0.3 eq.) was added, and the solution was stirred at room temperature for 24 h. Subsequently, unconjugated dye was removed by repetitive precipitation in THF (4500 rpm, 3 min, 4°C), as verified by HFIP-GPC. ^{1}H NMR (500 MHz, DMSO-*d*$_6$): δ (ppm) 8.77 (b s, 1mH, CON*H*), 4.72 (m, 1mH, α-C*H*$_{(L\text{-}Cys)}$), 4.50 - 3.79 (m, 2nH, -C*H*$_{2(Sar)}$), 3.54 (m, 4mH, -S-C*H*$_2$, -SO$_2$-C*H*$_2$), 3.06 - 2.61 (m, 3nH, -CH$_{3(Sar)}$), 1.29 (t, *J* = 7.3 Hz, 3mH, -CH$_{3(L\text{-}Cys)}$).

Cross-Linker Syntheses: The bifunctional cross-linker (*R*)-lipoic acid hydrazide (3) was synthesized in a two-step procedure following our previous report (Scheme S1).[51]

(R)-Methyl Lipoate: (*R*)-Methyl lipoate (2) was prepared according to our previous report and the synthesis was adapted and modified from Hassan and Maltman.[51,65] (*R*)-Lipoic acid (1) (4.00 g; 19.4 mmol; 1.0 eq.) was dissolved in dry methanol (12 mL), and sulfuric acid (10.3 µL; 194 µmol; 0.01 eq.) was added. The reaction mixture was stirred at room temperature for 18 h and protected from

light. A yellow solid precipitated after 30 minutes. The yellow suspension was concentrated *in vacuo*, and the crude was dissolved in dichloromethane. The organic phase was washed with $NaHCO_3$ solution (3x) and brine (3x), dried over $MgSO_4$, filtered, and concentrated *in vacuo*. (*R*)-Methyl lipoate (**2**) was obtained as a yellow oil (3.84 g; 17.4 mmol; 90%) and used without further purification. ^{1}H NMR (400 MHz, DMSO-d_6): δ (ppm) 3.62 (m, 1H, -S-C*H*), 3.58 (s, 3H, -OCH_3), 3.15 (m, 2H, -S-CH_2), 2.40 (m, 1H, -S-CH$_2$-CH_2), 2.33 (t, J = 7.5 Hz, 2H, α-CH_2), 1.87 (m, 1H, -S-CH$_2$-CH_2), 1.73–1.61 (m, 4H, ß-CH_2, δ-CH_2), 1.39 (m, 2H, γ-CH_2).

(R)-Lipoic Acid Hydrazide: (*R*)-Lipoic acid hydrazide (**3**) was synthesized following our previous report, and the synthesis was adapted and modified from Koufaki *et al.*[51,66] (*R*)-Methyl lipoate (**2**) (2.00 g; 9.04 mmol; 1.0 eq.) was dissolved methanol (10 mL), and hydrazine hydrate (1.33 mL; 27.1 mmol; 3.0 equiv) was added to the yellow solution. The reaction mixture was stirred at room temperature for 96 h in the absence of light. The solution was concentrated *in vacuo* and dissolved in chloroform. The organic layer was washed with brine (3x), dried with $MgSO_4$, filtered, and concentrated *in vacuo*. (*R*)-Lipoic acid hydrazide (**3**) was obtained as a yellow oil (1.50 g; 6.78 mmol; 75%) and used without further purification. ^{1}H NMR (400 MHz, DMSO-d_6): δ (ppm) 8.91 (b s, 1H, -CON*H*), 4.14 (b s, 2H, -NH-NH_2), 3.60 (m, 1H, -S-C*H*), 3.11 (m, 2H, -SCH_2), 2.40 (m, 1H, -S-CH$_2$CH_2), 2.00 (t, J = 7.3 Hz, 2H, α-CH_2), 1.87 (m, 1H, -S-CH$_2$CH_2), 1.60-1.43 (m, 4H, -ß-CH_2, δ-CH_2), 1.40-1.27 (m, 2H, γ-CH_2).

Solid Phase Peptide Synthesis

Resin loading: Fmoc-L-cysteine(Trt)-OH (2.0 eq. relative to the resin loading capacity) was dissolved in DCM (10 mL·g^{-1} resin), and a small amount of DMF was added to aid solvation. The vessel (Merryfield Apparatus) was charged with 2-chlorotrityl chloride resin and the dissolved Fmoc-L-cysteine(Trt)-OH and DIPEA (each 2.0 eq. relative to resin loading capacity) were added. The mixture was shaken for 5 min before additional DIPEA (3.0 eq.) was added and, the reaction mixture was shaken for 1 h at room temperature. Subsequently, MeOH (1 mL·g^{-1} resin) was added, and the reaction mixture was shaken for 15 min. Next, the vessel was drained and washed with 10 mL of DCM (3 x), DMF (3 x), DCM (3 x), and MeOH (3 x). The loaded resin was dried under high vacuum overnight.

Peptide Synthesis: The following steps were performed on a CS136XT peptide synthesizer (CSBio Ltd.). The loaded resin was placed in a reaction vessel and DCM was added to induce swelling. To cleave the Fmoc-group, the DCM was

removed, and a piperidine solution (20% in DMF) was added, and the vessel was shaken for 20 min. The reaction mixture was drained, and the beads were washed with DMF (4x) and DCM (2x). In the next step, a solution of a Fmoc-protected amino acid (4.0 eq. relative to the resin loading capacity) in DMF, HATU (4.0 eq.), and DIPEA (6.0 eq.) were added to the reaction vessel. The reaction mixture was shaken for 4 h. After the completed reaction the resin was washed with DMF (2x) and DCM (1x), followed by the deprotection procedure. The Fmoc-deprotection step and the coupling reactions were repeated with respect to the targeted amino acid sequence (NH-Cys-Sar-Cys-Sar-Cys).

Cleavage of the Peptide from the Resin: The resin-bound peptide was transferred from the reaction vessel of the peptide synthesizer to a Merryfield Apparatus. A mixture of trifluoroethanol and DCM (2:8; 30 mL) was added, and the beads were shaken for 1 h. The vessel was drained, washed with DCM, and the procedure was repeated two times. The obtained solutions were combined and concentrated *in vacuo*. The peptide was precipitated into cold cyclohexane/diethyl ether (2:1), centrifuged, and lyophilized.

Peptide Modification

N-tert-Butyloxycarbonyl-Succinic Acid Monohydrazide (Boc-Hydrazine): Succinic anhydride (6) (3.3 g; 33.0 mmol; 1.0 eq.) and Boc-hydrazine (5) (4.36 g; 33.0 mmol; 1.0 eq) were placed in a flask and suspended in H_2O (60 mL). After 30 min, the solution turned clear. The solution was lyophilized, and *N-tert*-butyloxycarbonyl-succinic acid monohydrazide (7) (7.63 g; 33.0 mmol; quant.) was obtained as a colorless solid. The product was used without any further purification. ^{1}H NMR (400 MHz, DMSO-d_6): δ (ppm) 11.85 (bs, 1H, -COO*H*), 9.53 (s, 1H, -N*H*COCH$_2$), 8.68 (s, 1H, -OCON*H*), 2.44-2.37 (m, 2H, -C*H*$_2$), 2.33-2.29 (m, 2H, -C*H*$_2$), 1.38 (s, 9H, -C*H*$_3$). ^{13}C NMR (101 MHz, DMSO-d_6): δ (ppm) 173.6 (-*C*OOH), 170.8 (-NH*C*OCH$_2$), 155.3 (-O*C*ONH), 83.6 (-*C*(CH$_3$)$_3$), 28.7 (-*C*H$_2$), 28.1 (-*C*H$_3$). ESI-HRMS (MeOH) (*m*/*z*): calculated for $[C_9H_{16}N_2O_5+H]^+$: 233.1132, found: 233.1136, calculated for $[C_9H_{16}N_2O_5+Na]^+$: 255.0951, found: 255.0958 .

Boc-Hydrazine-Cys(Trt)-Sar-Cys(Trt)-Sar-Cys(Trt)-OH: The peptide was synthesized according to the general procedures on SPPS with 1.72 g (1.6 mmol·g^{-1}; 2.75 mmol) resin. The crude product was purified through FC on silica gel (DCM:EtOAc = 1:1 to DCM:EtOAc:MeOH = 5:3:2). After freeze drying, the product (8) was obtained as a colorless solid. ^{1}H NMR (400 MHz, DMSO-d_6): δ (ppm) 12.81 (s, 1H, -COO*H*), 9.52 (s, 1H, -N*H*COCH$_2$), 8.68 (s, 1H, -OCON*H*), 8.60-8.55 (m, 1H, α-CHN*H*), 8.36-

8.20 (m, 2H, α-CHN*H*), 7.38-7.19 (m, 45H, -C$H_{arom.}$), 4.70-4.56 (m, 2H, α-C*H*), 4.26-3.60 (m, 5H, α-C*H*, α_{Sar}-CH_2), 2.72-2.62 (m, 6H, -NCH_3), 2.48 - 2.28 (m, 10H, -CH_2CH_2, -CH_2S), 1.39 (s, 9H, -(CH_3)$_3$). ESI-HRMS (MeOH) (*m*/*z*): calculated for $[C_{81}H_{83}N_7O_{10}S_3+Na]^+$: 1432.5256, found 1432.5254.

Boc-Hydrazine-Cys(Trt)-Sar-Cys(Trt)-Sar-Cys(Trt)-4-Fluorobenzylamine: Compound (8) (2.46 g; 1.74 mmol; 1.0 eq.) was dissolved in DMF (50 mL) and 4-fluorobenzylamine (654 mg; 5.22 mmol; 3.0 eq.), PyBOP (1.36 g; 2.61 mmol; 1.5 eq.), HOAt (237 mg; 1.74 mmol; 1.0 eq.) as well DIPEA (546 µL; 2.09 mmol; 1.2 eq.) were added. The reaction mixture was stirred overnight at RT. Further PyBOP (453 mg; 871 µmol; 0.5 eq.) and DIPEA (227 µl; 871 µmol; 0.5 eq.) were added and stirred for another two hours. The solvent was removed *in vacuo*, the crude was purified by SEC ($CHCl_3$:MeOH = 1:1) and the product (9) was obtained as a colorless solid (1.91 g; 1.74 mmol; 72%). ^{1}H NMR (400 MHz, DMSO-d_6): δ (ppm) = 9.52 (s, 1H, -N*H*COCH$_2$), 8.67 (s, 1H, -OCON*H*), 8.62-8.46 (m, 2H, αCH-N*H*), 8.35-8.17 (m, 2H, -N*H*CH$_2$), 7.33-7.19 (m, 47H, -C$H_{arom\text{-}Trityl,}$ -CH$_2$CCH_{arom}), 7.09-6.96 (m, 2H, -CH_{arom}CF), 4.69-4.55 (m, 2H, α-C*H*), 4.39-4.24 (m, 3H, α-C*H*, -NHCH_2), 4.06-3.62 (m, 4H, α_{Sar}-CH_2), 2.68-2.60 (m, 6H, -NCH_3), 2.43-2.17 (m, 10H, -CH_2CH_2, -CH_2S), 1.38 (s, 9H, -(CH_3)$_3$). ^{19}F NMR (376 MHz, DMSO-d_6): *δ* (ppm) = -117.4 (CH$_{arom}$C*F*). ESI-HRMS (MeOH) (*m*/*z*): calculated for $[C_{88}H_{89}FN_8O_9S_3+H]^+$: 1517.5971 found: 1517.5969; calculated for $[C_{88}H_{89}FN_8O_9S_3+Na]^+$: 1539.5791, found: 1539.5796.

Hydrazine-Cys-Sar-Cys-Sar-Cys-4-Fluorobenzylamine: The protecting groups of compound (9) (1.01 g; 663 µmol; 1.0 eq.) were cleaved from the peptide with a mixture of TFA:TIPS:H_2O:Ethanedithiol (94 : 1 : 2.5 : 2.5 = 5 ml). The reaction mixture was stirred for 90 min and in the meantime the solution turned yellow. Then the solution was precipitated in a cold mixture of diethyl ether and pentane (1:1), centrifuged, the pellet dried in high vacuum and freeze dried. Not all the cleaved protecting groups could be removed through precipitation, therefore the peptide was solved in water (10 mL) and extracted with diethyl ether (3 x 15 mL). The aqueous layer was lyophilized, and the protecting group-free product (10) was obtained as a colorless solid (392 mg, 488 µmol, 74%). ^{1}H NMR (600 MHz, DMSO-d_6): *δ* (ppm) 10.63 (s, 1H, -N*H*COCH$_2$), 8.66-8.64 (m, 0.5H, α-CHN*H*), 8.58-8.55 (m, 1H, α-CHN*H*), 8.49-8.46 (m, 0.5H, α-CHN*H*), 8.39-8.36 (m, 1H, α-CHN*H*), 8.29-8.19 (m, 1H, α-CHN*H*), 7.30-7.28 (m, 2H, -CH$_2$CCH_{arom}), 7.15-7.11 (m, 2H, -CH_{arom}CF), 4.90-4.78 (m, 1H, α-C*H*), 4.72-4.54 (m, 1H, α-C*H*), 4.44-4.34 (m, 2H, α-C*H*), 4.30-4.27 (m, 2H, -NHCH_2), 4.24-3.82 (m, 4H, α_{Sar}-CH_2), 3.08-3.02 (m, 4H,

n), 2.86-2.69 (m, 6H, -NCH_3), 2.62-2.52 (m, 4H, -CH_2CH_2), 2.47-2.24 (m, 6H, -CH_2S). ^{19}F NMR (376 MHz, DMSO-d_6): δ (ppm) -74.7 (CF_3), -117.4 ($CH_{arom}CF$). ESI-HRMS (MeOH) (*m/z*): calculated for $[C_{26}H_{40}FN_8O_7S_3+H]^+$: 691.2161 found: 691.2146; calculated for $[C_{88}H_{89}FN_8O_9S_3+Na]^+$: 713.198, found: 713.197.

Polymeric Micelles: The preparation of core cross-linked polymeric micelles (CCPMs) was adapted and modified from our previous reports.[50,51] Briefly, Atto 647N labeled pSar_{200}-*b*-p(L)Cys(SO_2Et)$_{17/30}$, was dissolved in DMSO (ß = 7.5 g·L^{-1}) equipped with 1 M thiourea. After 1 h, 20 vol.% 1 mM acetate buffer (pH 4.75) containing 10 mM thiourea was added, and the solution was left to equilibrate at room temperature for 4 h. The solution was placed into a dialysis bag and dialyzed with 1 mm acetate buffer (pH 4.75, 10 mM thiourea), and the solvent was changed 4 times. The solution was filtered by syringe filter (PVDF; 450 nm) and concentrated to 7 g·L^{-1} by spin filtration (Amicon Ultra; MWCO, 3 kDa), yielding the polymeric micelles (PMs). In a following step, the PMs were treated with (A) (*R*)-dihydrolipoic acid hydrazide (4) for 2F-$CL_{17/30}$, (B) the cys/sar pentapeptide (10) for 3F-$CL_{17/30}$, or (C) with methyl 3-mercaptopropionate for $NCL_{17/30}$ at equimolar amounts of thiols per *S*-ethylsulfonyl-L-cysteine.

For cross-linking with bifunctional (*R*)-dihydrolipoic acid hydrazide (4), (*R*)-lipoic acid hydrazide (3) was dissolved in ethanol at a concentration of ß = 20 g·L^{-1}, and 0.5 equivalents of tris(2-carboxyethyl)phosphine hydrochloride (TCEP·HCl) (ß = 50 g·L^{-1} in water) were added. After reaction for 18 h, the cross-linker solution (4) was added to the PMs. For cross-linking with trifunctional Cys/Sar pentapeptide (10), the cross-linker was dissolved in ethanol at a concentration of ß = 20 g·L^{-1} and added to the PMs. After 48 h of reaction, the CCPM solutions were dialyzed against DMSO/water mixtures (1/1; MWCO, 6-8 kDa) and water, followed by repetitive spin filtration (Amicon Ultra; MWCO, 100 kDa) to remove residual cross-linker and free polymer, as verified by HFIP-GPC.

For quenching with monofunctional methyl 3-mercaptopropionate, the thiol-reagent was dissolved in ethanol at a concentration of ß = 20 g·L^{-1} and added to the PMs. After 48 h of reaction, the NCL particles were dialyzed against ethanol/water mixtures (1/2; MWCO, 3 kDa) and water, followed by concentration via spin filtration (Amicon Ultra; MWCO, 3 kDa). The final particle concentrations were determined from lyophilization of aliquots.

AF4-Analysis: A 20-fold stock solution of the used phosphate buffered saline (PBS) was prepared out of sodium chloride, potassium chloride, disodium phosphate and

potassium phosphate with a final salt concentration of 151.7 mmol·L^{-1}, further containing 0.2 mmol·L^{-1} sodium azide. The stock solution was filtered (Millipore GHP 0.22 µm) before using it in the AF4 system. Human blood plasma was provided from the transfusion center of the Medical Department of the Johannes Gutenberg-University Mainz. It was pooled of six healthy donors and stabilized with EDTA.

The nanoparticles (30 g·L^{-1}) were incubated with EDTA-stabilized, pure and undiluted plasma 1:1 (v:v) at 37 °C for 1 h. For a sufficient separation the AF4 is limited to a maximal plasma concentration of 5 vol%. Therefore, after incubation time, the samples were diluted with PBS to a particle concentration of 1.5 g·L^{-1} corresponding to a 5 vol% solution of plasma in PBS. Samples were measured by AF4 immediately after preparation.

The AF4 measurements were performed using an installation from the ConSenxuS GmbH using a constaMETRICR 3200 main pump, a Spectra Series UV150 detector (Thermos Separation), a Dark V3 LS Detector (ConSenxuS GmbH), a Pharmacia P-3500 injection pump, a LV-F flow controller (HORIBA ATEC), and an In-Line Degasser-AF (Waters). A separation channel with a 190 µm spacer and a regenerated cellulose membrane with a molecular weight cut-off of 10 kDa suitable for protein separation was used.[67] The UV absorption was detected at 220 nm. For all measurements PBS (151.7 mM) containing 0.2 mmol·L^{-1} sodium azide was used as the solvent. The main flow was 1 mL·min^{-1} higher than the crossflow for every measurement. The crossflow is illustrated in the respective AF4 elugrams. Every nanoparticle was analyzed by at least three independent measurements performed *via* plasma independent incubation experiments.

FCS-Analysis: The FCS experiments was performed on a LSM 880 (Carl Zeiss, Jena, Germany) setup.[68] The excitation laser (He-Ne laser at 633 nm) was focused on the samples using a Zeiss C-Apochromat 40×/1.2 W water immersion objective. The fluorescence emission was collected with the same objective and directed to a spectral detection unit (Quasar, Carl Zeiss) after passing through a confocal pinhole. The fluorescence emission was spectrally separated by a grating element on a 32-channel array of GaAsP detectors operating in single photon counting mode. A detection range of 642–696 nm was used. An eight-well polystyrene-chambered cover glass (Nunc Lab-Tek, Thermo Fisher Scientific, Waltham, MA) was used as the sample cell. For each sample, a series of 15 measurements, 10 s

each, was performed at room temperature (23 °C). For experiments with human blood plasma, the samples were incubated with human blood plasma for 1 h at 37°C prior to the measurement. The obtained experimental autocorrelation curves were fitted with the following analytical model function:

$$G(\tau) = 1 + \frac{1}{N}\sum_{i=1}^{m} \frac{f_i}{\left(1 + \frac{\tau}{\tau_{D,i}}\right) \cdot \sqrt{1 + \frac{\tau}{S^2 \cdot \tau_{D,i}}}}$$

whereby N is the average number of diffusing fluorescencent species in the observation volume, τ_{Di} is the lateral diffusion time of the i-th species, f_i is the fraction of the component i ($1 \leq i \leq m$), and S is the structure parameter, $S = z_0/r_0$, where z_0 and r_0 represent the axial and radial dimensions of the observation volume. The diffusion coefficients of the species D_i are related to the respective diffusion times τ_{Di} and the radial dimension r_0 of V_{obs} by $D_i = r_0^2/(4\tau_{Di})$. By inserting D_i into the Stokes-Einstein equation, $R_h = \frac{k_B \cdot T}{6 \cdot \pi \cdot \eta \cdot D}$, we can calculate the hydrodynamic radius of the respective fluorescent species. Here, k_B is the Boltzmann constant, T is the temperature, and η is the viscosity of the solvent. As the value of r_0 depends on the optical setup, a calibration was performed using Alexa Fluor 647 (D = 330 μm² s⁻¹ at 25 °C) as reference standard with known diffusion coefficient.

Biologic Evaluation: All animal work was performed at the Leiden University animal facility and was approved by the Leiden University Animal Ethics Committee. The animal experiments were performed according to the guidelines from Dutch government guidelines and the Directive 2010/63/EU of the European Parliament on the protection of animals used for scientific purposes under the permit number AVD1060020187085.

Male C57Bl/6 mice, aged 13-17 weeks, were housed in individually ventilated cages under a constant 12 h light-dark cycle and maintained on a standard mouse diet. Prior to the experiment, mice were weighed and randomly allocated to the different groups using the randomization tool RandoMice with the weight as blocking factor for randomization. After 1 week of acclimatization, the mice received a single intravenous injection (200 μL) of Atto647N-labeled CCPMs in PBS (5 μg/μL) or PBS (control) through the tail vein. Blood samples of 50 μL were collected from the tail vein at the following time points after systemic administration: 10 min, 1 h, 6 h, 24 h, 72 h. EDTA-treated Eppendorf tubes were applied to prevent blood clotting and kept at 4 °C. For fluorescence quantification,

blood cells were separated by centrifugation (Mikro 200R, Andreas Hettich GmbH & Co KG) (1000 rpm, 10 min, 4°C) and 25 µL of the supernatant were transferred into a transparent 96-well plate (Greiner Bio-one, The Netherlands) and diluted with 75 µL of PBS. The particle fluorescence was quantified by Tecan Spark plate reader (Tecan Group Ltd.) at an emission wavelength of 640 nm and detection wavelength of 670 nm at a fixed gain of 200 and a bandwidth of 5 nm. The fraction of particles in circulation for each time point was calculated as:

$$CCPMs\ in\ circulation = \frac{(fluorescence_{CCPM}(t = x) - fluorescence_{PBS})}{(fluorescence_{CCPM}\ (t = 0) - fluorescence_{PBS})}$$

The values obtained at t = 10 min were considered as 100% value.

At post-administration 72 h, mice were euthanized, and after perfusion the organs were collected and analyzed by ex vivo fluorescence analysis. Lungs, liver, spleen, kidneys, heart, and small intestine were collected, and kept in a 6-well plate under PBS stored on ice. The fluorescence per organ was measured on an IVIS Spectrum (Perkin Elmer, Massachusetts, USA) using the IS0709N4132 camera (Spectral Instruments TE) at an excitation wavelength of 605 nm and a detection wavelength of 680 nm. Image acquisition and analysis was performed with Living Image (version 4.7.2; Perkin Elmer). For normalization, the total fluorescence intensity was divided by the fluorescent area or the respective organ weight.

Author Contribution

Experimental design, polymer synthesis, nanoparticle preparation, DLS measurements, NP-fluorescence quantification in blood samples, and statistical analysis were performed by T.A.B., I.A. executed AF4 analyses, L.A.Z. synthesized the trifunctional peptide cross-linker. H.Z. supervised IVIS imaging, K.K. contributed FCS analysis, and B.S. performed the *in vivo* experiments. The manuscript was written by T.A.B. and M.B. The project was supervised by R.Z. and M.B.

Notes

The authors declare the following competing financial interest(s): Matthias Barz holds the patent Thiol-protected amino acid derivatives and uses thereof WO2015169908A1.

Acknowledgement

We would like to thank Mireia Bernabé Klein for supporting the in vivo study and Ivo Que for IVIS measurements. T.A.B, I.A., K.K., P.B., R.Z., and M.B. would like to acknowledge the Deutsche Forschungsgemeinschaft (SFB1066) for funding. T.A.B. acknowledge the HaVo Foundation and the Max-Planck-Graduate-Center for financial support. L.A.Z. thanks the Evonik Foundation (Werner Schwarze Scholarship) for financial support.

References

(1) Zhang, C.; Yan, L.; Wang, X.; Zhu, S.; Chen, C.; Gu, Z.; Zhao, Y. Progress, Challenges, and Future of Nanomedicine. *Nano Today* **2020**, *35*.

(2) Cabral, H.; Miyata, K.; Osada, K.; Kataoka, K. Block Copolymer Micelles in Nanomedicine Applications. *Chem. Rev.* **2018**, *118* (14), 6844–6892.

(3) Duncan, R. The Dawning Era of Polymer Therapeutics. *Nat. Rev. Drug Discov.* **2003**, *2* (5), 347–360.

(4) Chan, W. C. W. Nanomedicine 2.0. *Acc. Chem. Res.* **2017**, *50* (3), 627–632.

(5) Bertrand, N.; Leroux, J. C. The Journey of a Drug-Carrier in the Body: An Anatomo-Physiological Perspective. *J. Control. Release* **2012**, *161* (2), 152–163.

(6) Talelli, M.; Barz, M.; Rijcken, C. J. F. F.; Kiessling, F.; Hennink, W. E.; Lammers, T. Core-Crosslinked Polymeric Micelles: Principles, Preparation, Biomedical Applications and Clinical Translation. *Nano Today* **2015**, *10* (1), 93–117.

(7) Shi, Y.; Van Steenbergen, M. J.; Teunissen, E. A.; Novo, L.; Gradmann, S.; Baldus, M.; Van Nostrum, C. F.; Hennink, W. E. Π-Π Stacking Increases the Stability and Loading Capacity of Thermosensitive Polymeric Micelles for Chemotherapeutic Drugs. *Biomacromolecules* **2013**, *14* (6), 1826–1837.

(8) Talelli, M.; Rijcken, C. J. F.; Hennink, W. E.; Lammers, T. Polymeric Micelles for Cancer Therapy: 3 C's to Enhance Efficacy. *Curr. Opin. Solid State Mater. Sci.* **2012**, *16* (6), 302–309.

(9) Lu, J.; Owen, S. C.; Shoichet, M. S. Stability of Self-Assembled Polymeric Micelles in Serum. *Macromolecules* **2011**, *44* (15), 6002–6008.

(10) Muhammad, N.; Guo, Z. Metal-Based Anticancer Chemotherapeutic Agents. *Curr. Opin. Chem. Biol.* **2014**, *19* (1), 144–153.

(11) Nishiyama, N.; Kato, Y.; Sugiyama, Y.; Kataoka, K. Cisplatin-Loaded Polymer-Metal Complex Micelle with Time-Modulated Decaying Property as a Novel Drug Delivery System. *Pharm. Res.* **2001**, *18* (7), 1035–1041.

(12) Bauer, T. A.; Eckrich, J.; Wiesmann, N.; Kuczelinis, F.; Sun, W.; Zeng, X.; Weber, B.; Wu, S.; Bings, N. H.; Strieth, S.; Barz, M. Photocleavable Core Cross-Linked Polymeric Micelles of Polypept(o)ides and Ruthenium(II) Complexes. *J. Mater. Chem. B* **2021**, 9, 8211-8223.

(13) Endo, K.; Ueno, T.; Kondo, S.; Wakisaka, N.; Murono, S.; Ito, M.; Kataoka, K.; Kato, Y.; Yoshizaki, T. Tumor-Targeted Chemotherapy with the Nanopolymer-Based Drug NC-6004 for Oral Squamous Cell Carcinoma. *Cancer Sci.* **2013**, *104* (3), 369–

374.

(14) Hu, Q.; Rijcken, C. J.; Bansal, R.; Hennink, W. E.; Storm, G.; Prakash, J. Complete Regression of Breast Tumour with a Single Dose of Docetaxel-Entrapped Core-Cross-Linked Polymeric Micelles. *Biomaterials* **2015**, *53*, 370–378.

(15) Van Driessche, A.; Kocere, A.; Everaert, H.; Nuhn, L.; Van Herck, S.; Griffiths, G.; Fenaroli, F.; De Geest, B. G. PH-Sensitive Hydrazone-Linked Doxorubicin Nanogels via Polymeric-Activated Ester Scaffolds: Synthesis, Assembly, and in Vitro and in Vivo Evaluation in Tumor-Bearing Zebrafish. *Chem. Mater.* **2018**, *30* (23), 8587–8596.

(16) Alberg, I.; Kramer, S.; Leps, C.; Tenzer, S.; Zentel, R. Effect of Core-Crosslinking on Protein Corona Formation on Polymeric Micelles. *Macromol. Biosci.* **2021**, *2000414*.

(17) Talelli, M.; Barz, M.; Rijcken, C. J. F. F.; Kiessling, F.; Hennink, W. E.; Lammers, T. Core-Crosslinked Polymeric Micelles: Principles, Preparation, Biomedical Applications and Clinical Translation. *Nano Today* **2015**, *10* (1), 93–117.

(18) Cabral, H.; Kataoka, K. Progress of Drug-Loaded Polymeric Micelles into Clinical Studies. *J. Control. Release* **2014**, *190*, 465–476.

(19) Mi, P.; Miyata, K.; Kataoka, K.; Cabral, H. Clinical Translation of Self-Assembled Cancer Nanomedicines. *Adv. Ther.* **2021**, *4* (1), 2000159.

(20) Atrafi, F.; Dumez, H.; Mathijssen, R. H. J.; Menke van der Houven van Oordt, C. W.; Rijcken, C. J. F.; Hanssen, R.; Eskens, F. A. L. M.; Schöffski, P. A Phase I Dose-Escalation and Pharmacokinetic Study of a Micellar Nanoparticle with Entrapped Docetaxel (CPC634) in Patients with Advanced Solid Tumours. *J. Control. Release* **2020**, *325* (March), 191–197.

(21) Sevier, C. S.; Kaiser, C. A. Formation and Transfer of Disulphide Bonds in Living Cells. *Nat. Rev. Mol. Cell Biol.* **2002**, *3* (11), 836–847.

(22) Schäfer, O.; Huesmann, D.; Muhl, C.; Barz, M. Rethinking Cysteine Protective Groups: S -Alkylsulfonyl- l -Cysteines for Chemoselective Disulfide Formation. *Chem. - A Eur. J.* **2016**, *22* (50), 18085–18091.

(23) Huesmann, D.; Schäfer, O.; Braun, L.; Klinker, K.; Reuter, T.; Barz, M. Exploring New Activating Groups for Reactive Cysteine NCAs. *Tetrahedron Lett.* **2016**, *57* (10), 1138–1142.

(24) Li, Y.; Xiao, K.; Luo, J.; Xiao, W.; Lee, J. S.; Gonik, A. M.; Kato, J.; Dong, T. A.; Lam, K. S. Well-Defined, Reversible Disulfide Cross-Linked Micelles for on-Demand Paclitaxel Delivery. *Biomaterials* **2011**, *32* (27), 6633–6645.

(25) Schäfer, O.; Barz, M. Of Thiols and Disulfides: Methods for Chemoselective Formation of Asymmetric Disulfides in Synthetic Peptides and Polymers. *Chem. - A Eur. J.* **2018**, *24* (47), 12131–12142.

(26) Bauer, T. A.; Muhl, C.; Schollmeyer, D.; Barz, M. Racemic S -(Ethylsulfonyl)- Dl -cysteine N -Carboxyanhydrides Improve Chain Lengths and Monomer Conversion for B-Sheet-Controlled Ring-Opening Polymerization. *Macromol. Rapid Commun.* **2021**, *42* (8), 2000470.

(27) Muhl, C.; Schäfer, O.; Bauer, T.; Räder, H.-J.; Barz, M. Poly(S -Ethylsulfonyl- l -Homocysteine): An α-Helical Polypeptide for Chemoselective Disulfide Formation. *Macromolecules* **2018**, *51* (20), 8188–8196.

(28) Schäfer, O.; Huesmann, D.; Barz, M. Poly(S -Ethylsulfonyl- l -Cysteines) for

Chemoselective Disulfide Formation. *Macromolecules* **2016**, *49* (21), 8146–8153.

(29) Klinker, K.; Barz, M. Polypept(o)ides: Hybrid Systems Based on Polypeptides and Polypeptoids. *Macromol. Rapid Commun.* **2015**, *36* (22), 1943–1957.

(30) Birke, A.; Huesmann, D.; Kelsch, A.; Weilbächer, M.; Xie, J.; Bros, M.; Bopp, T.; Becker, C.; Landfester, K.; Barz, M. Polypeptoid- Block -Polypeptide Copolymers: Synthesis, Characterization, and Application of Amphiphilic Block Copolypept(o)Ides in Drug Formulations and Miniemulsion Techniques. *Biomacromolecules* **2014**, *15* (2), 548–557.

(31) Weber, B.; Birke, A.; Fischer, K.; Schmidt, M.; Barz, M. Solution Properties of Polysarcosine: From Absolute and Relative Molar Mass Determinations to Complement Activation. *Macromolecules* **2018**, *51* (7), 2653–2661.

(32) Ostuni, E.; Chapman, R. G.; Holmlin, R. E.; Takayama, S.; Whitesides, G. M. A Survey of Structure-Property Relationships of Surfaces That Resist the Adsorption of Protein. *Langmuir* **2001**, *17* (18), 5605–5620.

(33) Son, K.; Ueda, M.; Taguchi, K.; Maruyama, T.; Takeoka, S.; Ito, Y. Evasion of the Accelerated Blood Clearance Phenomenon by Polysarcosine Coating of Liposomes. *J. Control. Release* **2020**, *322* (March), 209–216.

(34) Nogueira, S. S.; Schlegel, A.; Maxeiner, K.; Weber, B.; Barz, M.; Schroer, M. A.; Blanchet, C. E.; Svergun, D. I.; Ramishetti, S.; Peer, D.; Langguth, P.; Sahin, U.; Haas, H. Polysarcosine-Functionalized Lipid Nanoparticles for Therapeutic MRNA Delivery. *ACS Appl. Nano Mater.* **2020**, *3* (11), 10634–10645.

(35) Ishida, T.; Ichihara, M.; Wang, X.; Yamamoto, K.; Kimura, J.; Majima, E.; Kiwada, H. Injection of PEGylated Liposomes in Rats Elicits PEG-Specific IgM, Which Is Responsible for Rapid Elimination of a Second Dose of PEGylated Liposomes. *J. Control. Release* **2006**, *112* (1), 15–25.

(36) Huesmann, D.; Sevenich, A.; Weber, B.; Barz, M. A Head-to-Head Comparison of Poly(Sarcosine) and Poly(Ethylene Glycol) in Peptidic, Amphiphilic Block Copolymers. *Polym. (United Kingdom)* **2015**, *67*, 240–248.

(37) Bleher, S.; Buck, J.; Muhl, C.; Sieber, S.; Barnert, S.; Witzigmann, D.; Huwyler, J.; Barz, M.; Süss, R. Poly(Sarcosine) Surface Modification Imparts Stealth-Like Properties to Liposomes. *Small* **2019**, *15* (50), 1–10.

(38) Mahmoudi, M.; Bertrand, N.; Zope, H.; Farokhzad, O. C. Emerging Understanding of the Protein Corona at the Nano-Bio Interfaces. *Nano Today* **2016**, *11* (6), 817–832.

(39) Schöttler, S.; Landfester, K.; Mailänder, V. Controlling the Stealth Effect of Nanocarriers through Understanding the Protein Corona. *Angew. Chemie - Int. Ed.* **2016**, *55* (31), 8806–8815.

(40) Alberg, I.; Kramer, S.; Schinnerer, M.; Hu, Q.; Seidl, C.; Leps, C.; Drude, N.; Möckel, D.; Rijcken, C.; Lammers, T.; Diken, M.; Maskos, M.; Morsbach, S.; Landfester, K.; Tenzer, S.; Barz, M.; Zentel, R. Polymeric Nanoparticles with Neglectable Protein Corona. *Small* **2020**, *16* (18), 1907574.

(41) Kappel, C.; Seidl, C.; Medina-Montano, C.; Schinnerer, M.; Alberg, I.; Leps, C.; Sohl, J.; Hartmann, A.-K.; Fichter, M.; Kuske, M.; Schunke, J.; Kuhn, G.; Tubbe, I.; Paßlick, D.; Hobernik, D.; Bent, R.; Haas, K.; Montermann, E.; Walzer, K.; Diken, M.; Schmidt, M.; Zentel, R.; Nuhn, L.; Schild, H.; Tenzer, S.; Mailänder, V.; Barz,

M.; Bros, M.; Grabbe, S. Density of Conjugated Antibody Determines the Extent of Fc Receptor Dependent Capture of Nanoparticles by Liver Sinusoidal Endothelial Cells. *ACS Nano* **2021**, *15*, 15191-15209.

(42) Kokkinopoulou, M.; Simon, J.; Landfester, K.; Mailänder, V.; Lieberwirth, I. Visualization of the Protein Corona: Towards a Biomolecular Understanding of Nanoparticle-Cell-Interactions. *Nanoscale* **2017**, *9* (25), 8858–8870.

(43) Docter, D.; Distler, U.; Storck, W.; Kuharev, J.; Wünsch, D.; Hahlbrock, A.; Knauer, S. K.; Tenzer, S.; Stauber, R. H. Quantitative Profiling of the Protein Coronas That Form around Nanoparticles. *Nat. Protoc.* **2014**, *9* (9), 2030–2044.

(44) Richtering, W.; Alberg, I.; Zentel, R. Nanoparticles in the Biological Context: Surface Morphology and Protein Corona Formation. *Small* **2020**, *16* (39), 1–8.

(45) Giddings, J. C. A New Separation Concept Based on a Coupling of Concentration and Flow Nonuniformities. *Sep. Sci.* **1966**, *1* (1), 123–125.

(46) Giddings, J. C. Field-Flow Fractionation: Analysis of Macromolecular, Colloidal, and Particulate Materials. *Science* **1993**, *260* (5113), 1456–1465.

(47) Bresseleers, J.; Bagheri, M.; Lebleu, C.; Lecommandoux, S.; Sandre, O.; Pijpers, I. A. B.; Mason, A. F.; Meeuwissen, S.; van Nostrum, C. F.; Hennink, W. E.; van Hest, J. C. M. Tuning Size and Morphology of Mpeg-b-p(Hpma-Bz) Copolymer Self-Assemblies Using Microfluidics. *Polymers (Basel).* **2020**, *12* (11), 1–18.

(48) Rijcken, C. J.; Snel, C. J.; Schiffelers, R. M.; van Nostrum, C. F.; Hennink, W. E. Hydrolysable Core-Crosslinked Thermosensitive Polymeric Micelles: Synthesis, Characterisation and in Vivo Studies. *Biomaterials* **2007**, *28* (36), 5581–5593.

(49) Dal, N. K.; Kocere, A.; Wohlmann, J.; Van Herck, S.; Bauer, T. A.; Resseguier, J.; Bagherifam, S.; Hyldmo, H.; Barz, M.; De Geest, B. G.; Fenaroli, F. Zebrafish Embryos Allow Prediction of Nanoparticle Circulation Times in Mice and Facilitate Quantification of Nanoparticle–Cell Interactions. *Small* **2020**, *16* (5), 1906719.

(50) Klinker, K.; Schäfer, O.; Huesmann, D.; Bauer, T.; Capelôa, L.; Braun, L.; Stergiou, N.; Schinnerer, M.; Dirisala, A.; Miyata, K.; Osada, K.; Cabral, H.; Kataoka, K.; Barz, M. Secondary-Structure-Driven Self-Assembly of Reactive Polypept(o)Ides: Controlling Size, Shape, and Function of Core Cross-Linked Nanostructures. *Angew. Chemie Int. Ed.* **2017**, *56* (32), 9608–9613.

(51) Bauer, T. A.; Imschweiler, J.; Muhl, C.; Weber, B.; Barz, M. Secondary Structure-Driven Self-Assembly of Thiol-Reactive Polypept(o)Ides. *Biomacromolecules* **2021**, *22* (5), 2171–2180.

(52) Hofmann, D.; Messerschmidt, C.; Bannwarth, M. B.; Landfester, K.; Mailänder, V. Drug Delivery without Nanoparticle Uptake: Delivery by a Kiss-and-Run Mechanism on the Cell Membrane. *Chem. Commun.* **2014**, *50* (11), 1369–1371.

(53) Quader, S.; Liu, X.; Toh, K.; Su, Y. L.; Maity, A. R.; Tao, A.; Paraiso, W. K. D.; Mochida, Y.; Kinoh, H.; Cabral, H.; Kataoka, K. Supramolecularly Enabled PH-Triggered Drug Action at Tumor Microenvironment Potentiates Nanomedicine Efficacy against Glioblastoma. *Biomaterials* **2021**, *267*, 120463.

(54) Talelli, M.; Iman, M.; Varkouhi, A. K.; Rijcken, C. J. F.; Schiffelers, R. M.; Etrych, T.; Ulbrich, K.; van Nostrum, C. F.; Lammers, T.; Storm, G.; Hennink, W. E. Core-Crosslinked Polymeric Micelles with Controlled Release of Covalently Entrapped Doxorubicin. *Biomaterials* **2010**, *31* (30), 7797–7804.

(55) Berger, A.; Noguchi, J.; Katchalski, E. Poly-L-Cysteine. *J. Am. Chem. Soc.* **1956**, *78* (17), 4483–4488.

(56) Zhang, X.; Waymouth, R. M. 1,2-Dithiolane-Derived Dynamic, Covalent Materials: Cooperative Self-Assembly and Reversible Cross-Linking. *J. Am. Chem. Soc.* **2017**, *139* (10), 3822–3833.

(57) Bauer, T. A.; Horvat, N. K.; Marques, O.; Chocarro, S.; Mertens, C.; Colucci, S.; Schmitt, S.; Carrella, L. M.; Morsbach, S.; Koynov, K.; Fenaroli, F.; Blümler, P.; Jung, M.; Sotillo, R.; Hentze, M. W.; Muckenthaler, M. U.; Barz, M. Core Cross-Linked Polymeric Micelles for Specific Iron Delivery: Inducing Sterile Inflammation in Macrophages. *Adv. Healthc. Mater.* **2021**, *2100385* (19), 2100385.

(58) Koynov, K.; Butt, H. J. Fluorescence Correlation Spectroscopy in Colloid and Interface Science. *Curr. Opin. Colloid Interface Sci.* **2012**, *17* (6), 377–387.

(59) Negwer, I.; Best, A.; Schinnerer, M.; Schäfer, O.; Capeloa, L.; Wagner, M.; Schmidt, M.; Mailänder, V.; Helm, M.; Barz, M.; Butt, H. J.; Koynov, K. Monitoring Drug Nanocarriers in Human Blood by Near-Infrared Fluorescence Correlation Spectroscopy. *Nat. Commun.* **2018**, *9* (1).

(60) Holm, R.; Douverne, M.; Weber, B.; Bauer, T.; Best, A.; Ahlers, P.; Koynov, K.; Besenius, P.; Barz, M. Impact of Branching on the Solution Behavior and Serum Stability of Starlike Block Copolymers. *Biomacromolecules* **2019**, *20* (1), 375–388.

(61) Maeda, H. Macromolecular Therapeutics in Cancer Treatment: The EPR Effect and Beyond. *J. Control. Release* **2012**, *164* (2), 138–144.

(62) Barenholz, Y. Doxil® - The First FDA-Approved Nano-Drug: Lessons Learned. *J. Control. Release* **2012**, *160* (2), 117–134.

(63) Shi, Y.; Lammers, T.; Storm, G.; Hennink, W. E. Physico-Chemical Strategies to Enhance Stability and Drug Retention of Polymeric Micelles for Tumor-Targeted Drug Delivery. *Macromol. Biosci.* **2016**, 1–11.

(64) Talelli, M.; Barz, M.; Rijcken, C. J. F. F.; Kiessling, F.; Hennink, W. E.; Lammers, T. Core-Crosslinked Polymeric Micelles: Principles, Preparation, Biomedical Applications and Clinical Translation. *Nano Today* **2015**, *10* (1), 93–117.

(65) Hassan, H. M. A.; Maltman, B. A. Mixed SAMs and MALDI-ToF MS: Preparation of N-Glycosylamine Derivative and Thioctic Acid Methyl Ester Bearing 1,2-Dithiolane Groups and Detection of Enzymatic Reaction on Au. *Bioorg. Chem.* **2012**, *40* (1), 6–9.

(66) Koufaki, M.; Kiziridi, C.; Alexi, X.; Alexis, M. N. Design and Synthesis of Novel Neuroprotective 1,2-Dithiolane/Chroman Hybrids. *Bioorg. Med. Chem.* **2009**, *17* (17), 6432–6441.

(67) Marioli, M.; Kok, W. T. Recovery, Overloading, and Protein Interactions in Asymmetrical Flow Field-Flow Fractionation. *Anal. Bioanal. Chem.* **2019**, *411* (11), 2327–2338.

(68) Rigler, R.; Wennmalm, S.; Edman, L. *FCS in Single Molecule Analysis*; Springer-Verlag: Berlin, 2001.

Supporting Information

Results and Discussion

Polymer Synthesis

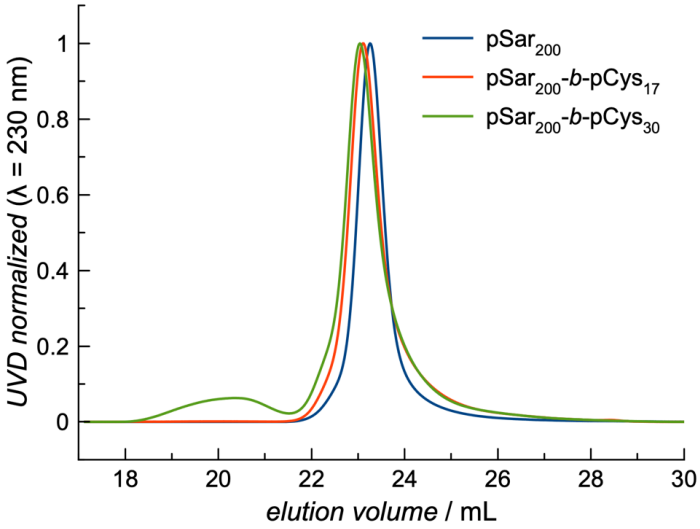

Figure S1. Analytical HFIP GPC of polypept(o)ides. Of note, secondary structure formation (anti-parallel ß-sheet) is not suppressed in HFIP accounting for the broad PDI of copolymers with increasing chain length of p(L)Cys(SO_2Et).

Table S1. Characterization of core cross-linked polymeric micelles with and without embedded iron oxide nanoparticles.

polymer	X_n pSar[a]	X_n pCys(SO_2Et)[b]	M_n[c]	$Đ$[c]
P1, $pSar_{200}$	200	-	40.9 kg·mol^{-1}	1.17
P2, $pSar_{200}$-*b*-$pCys(SO_2Et)_{17}$	200	17	40.9 kg·mol^{-1}	1.19
P3, $pSar_{200}$-*b*-$pCys(SO_2Et)_{17}$	200	30	40.9 kg·mol^{-1}	2.52

[a] HFIP-GPC relative to pSar standards. [b] determined by ^{1}H NMR. [c] HFIP-GPC releative to PMMA standards; secondary structure formation of p(L)Cys(SO2Et) is not suppressed accounting for broad dispersities.

Cross-Linker Synthesis

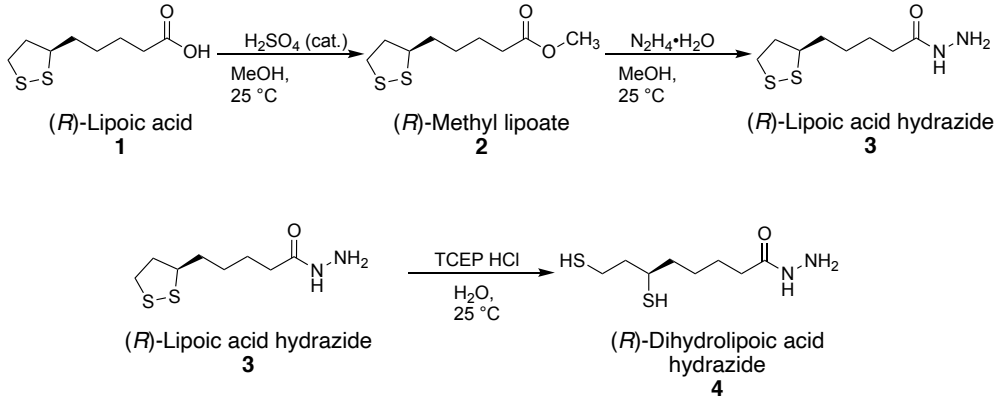

Scheme S1. Synthetic pathway to the bifunctional lipoic acid hydrazide (**4**) cross-linker.

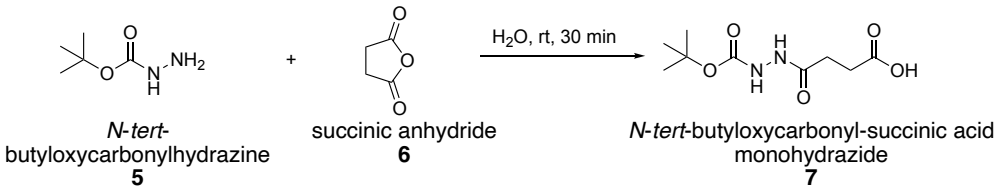

Scheme S2. Synthetic pathway to the N-tert-butyloxycarbonyl-succinic acid monohydrazide (**7**).

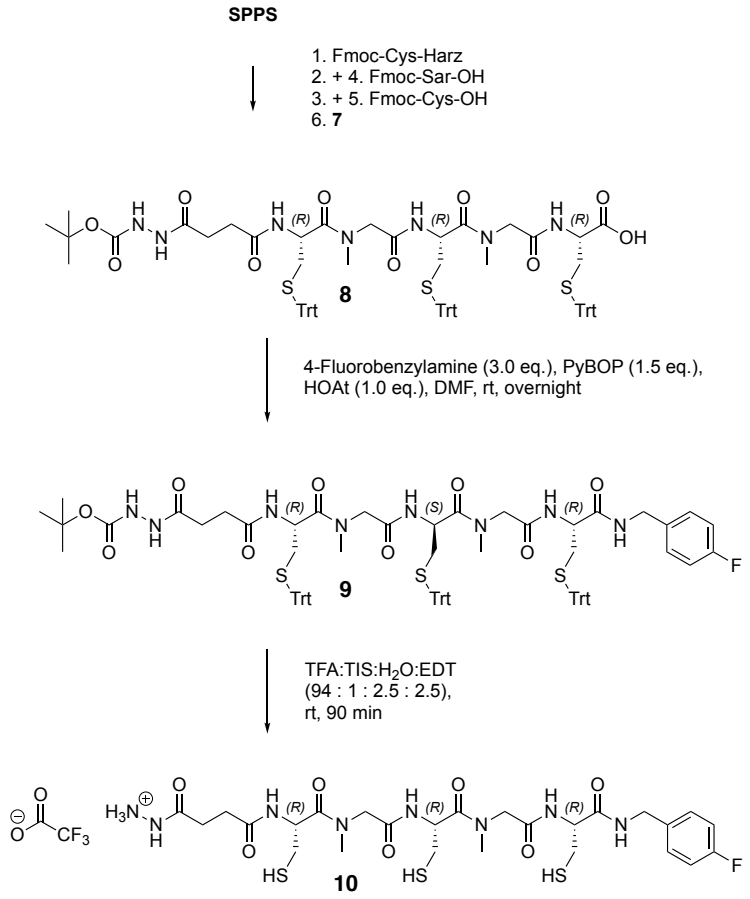

Scheme S3. Synthetic pathway to the trifunctional pentapeptide cross-linker **10** via solid-phase peptide synthesis.

Particle Synthesis

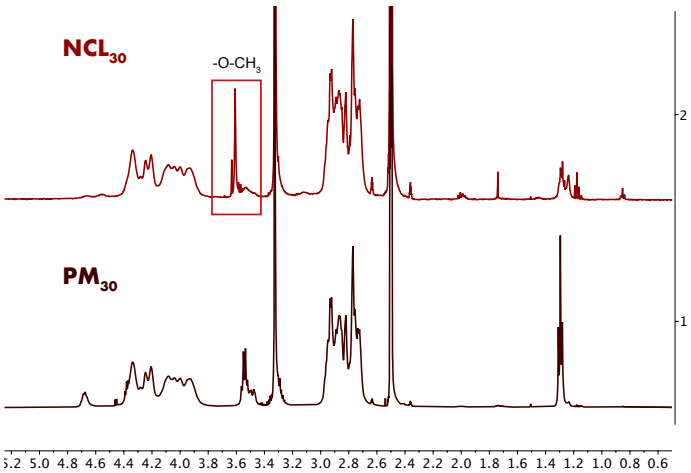

Figure S2. NMR analysis of the polymeric micelles before (PM_{30}) and after quenching of the *S*-ethylsulfonyl group with methyl 3-mercaptopropionate (NCL_{30}). For NCL_{30}, no signals of the *S*-ethylsulfonyl group but only signals of the methoxy group can be detected indicating complete removal of the reactive group.

Ex vivo Imaging

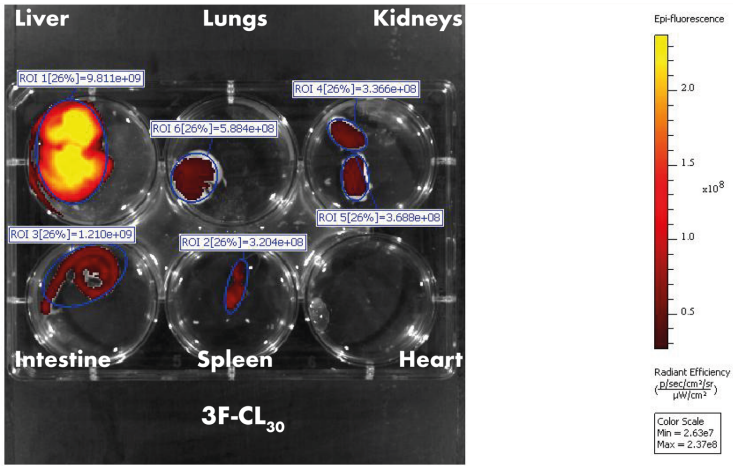

Figure S3. Ex vivo organ imaging by IVIS Spectrum (Perkin Elmer, Massachusetts, USA) shown for a representative mouse treated with 3F-CL_{30}. Fluorescence associated to the intestine originates from the diet.

NMR-Data

Polypept(o)ides

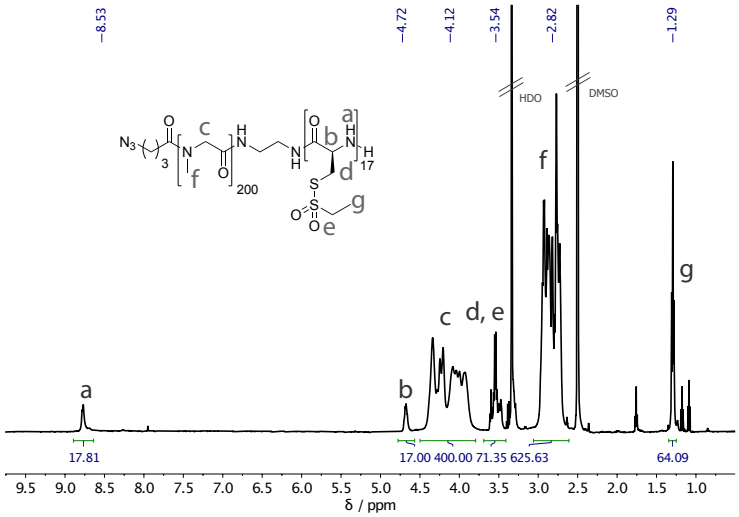

Figure S4. ^{1}H NMR of pSar$_{200}$-*b*-p(L)Cys(SO$_2$Et)$_{17}$ in DMSO-d_6.

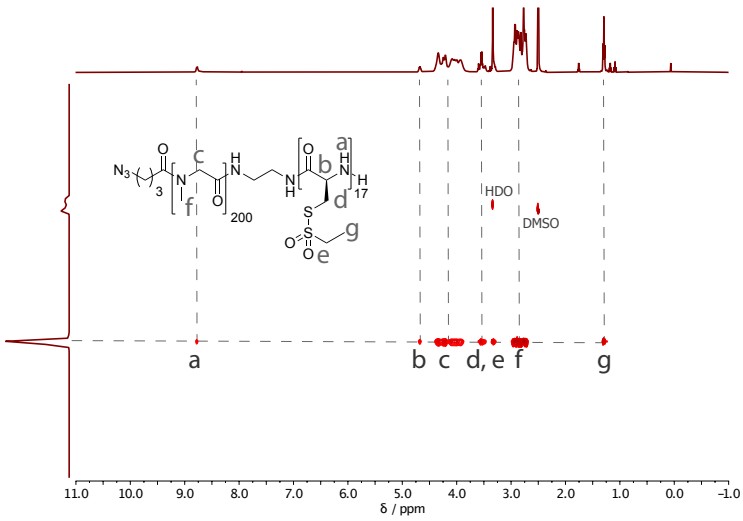

Figure S5. DOSY NMR analysis of pSar$_{200}$-*b*-p(L)Cys(SO$_2$Et)$_{17}$ in DMSO-d_6.

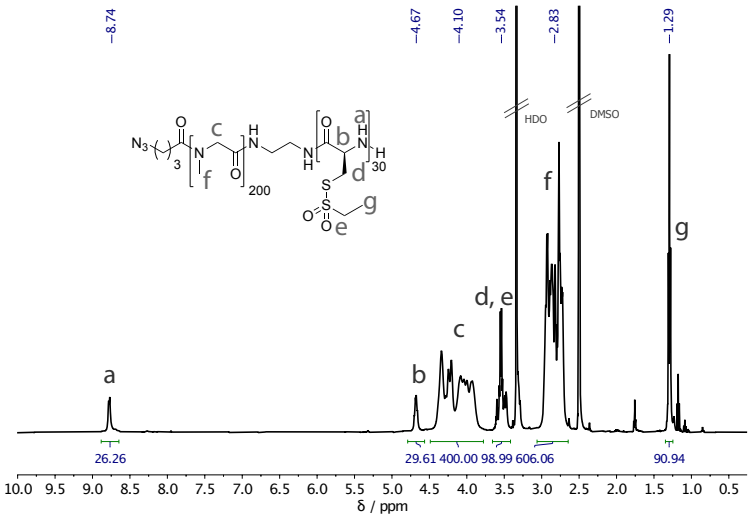

Figure S6. ^{1}H NMR of pSar$_{200}$-*b*-p(L)Cys(SO$_2$Et)$_{27}$ in DMSO-d_6.

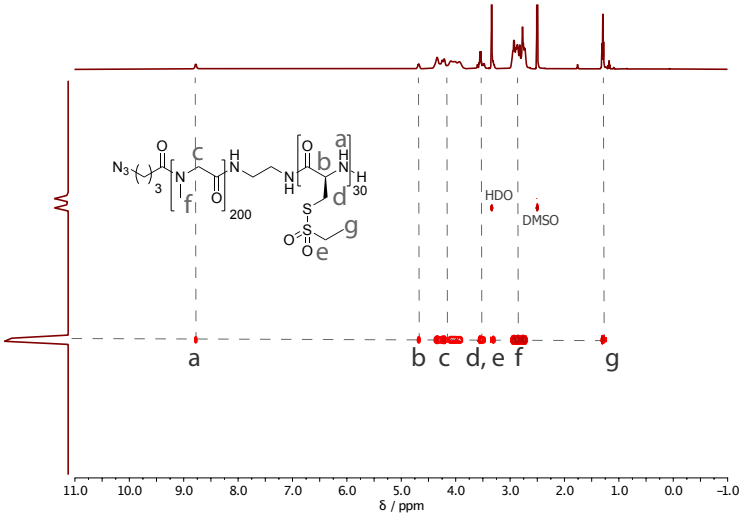

Figure S7. DOSY NMR analysis of pSar$_{200}$-*b*-p(L)Cys(SO$_2$Et)$_{27}$ in DMSO-d_6.

Peptide Cross-Linker

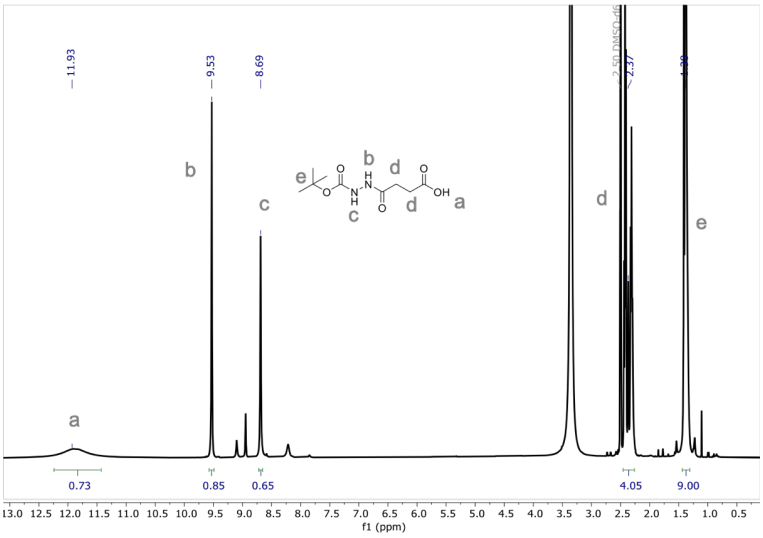

Figure S8. ^{1}H NMR of *N-tert*-butyloxycarbonyl-succinic acid monohydrazide (**7**) in DMSO-d_6.

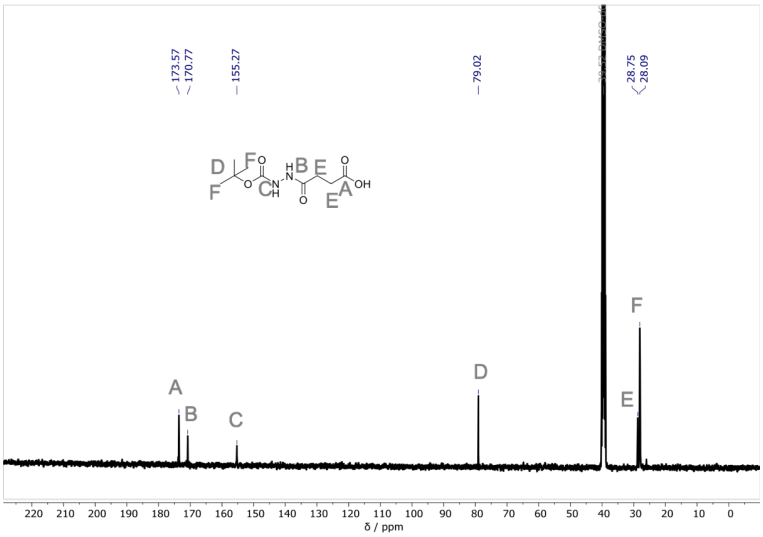

Figure S9. ^{13}C NMR of *N-tert*-butyloxycarbonyl-succinic acid monohydrazide (7) in DMSO-d_6.

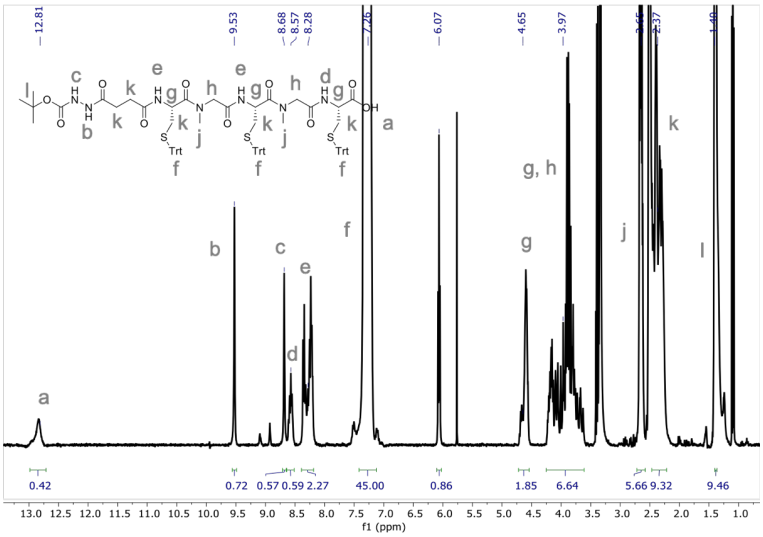

Figure S10. ^{1}H NMR of Boc-hydrazine-Cys(Trt)-Sar-Cys(Trt)-Sar-Cys(Trt)-OH (8) in DMSO-*d*$_6$.

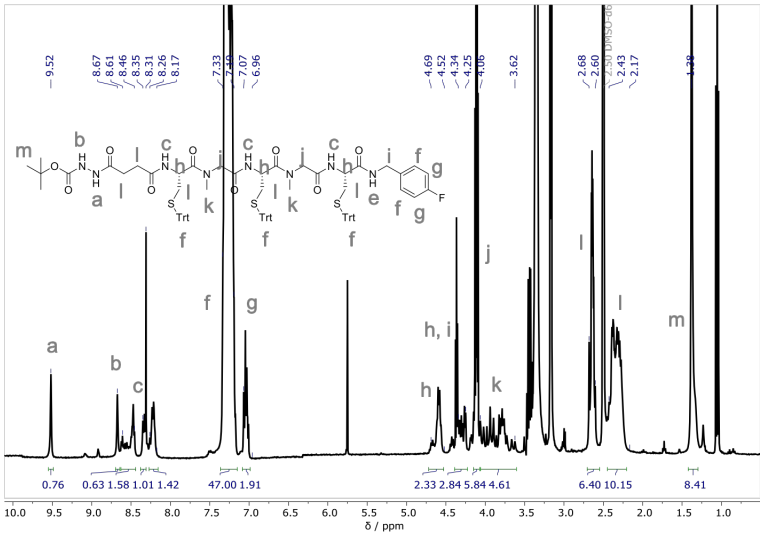

Figure S11. ^{1}H NMR of Boc-hydrazine-Cys(Trt)-Sar-Cys(Trt)-Sar-Cys(Trt)-(4-fluorobenzylamine) (9) in DMSO-*d*$_6$.

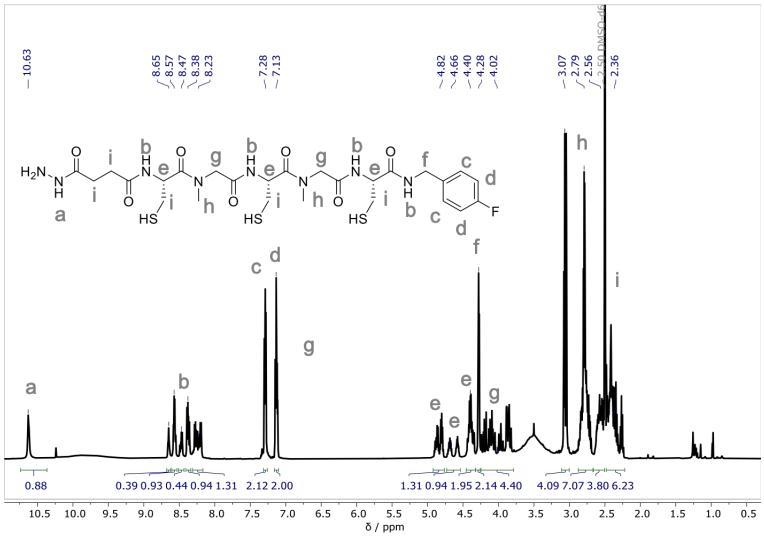

Figure S12. ^{1}H NMR of hydrazine-Cys-Sar-Cys-Sar-Cys-(4-fluorobenzylamine) (10) in DMSO-d_6.

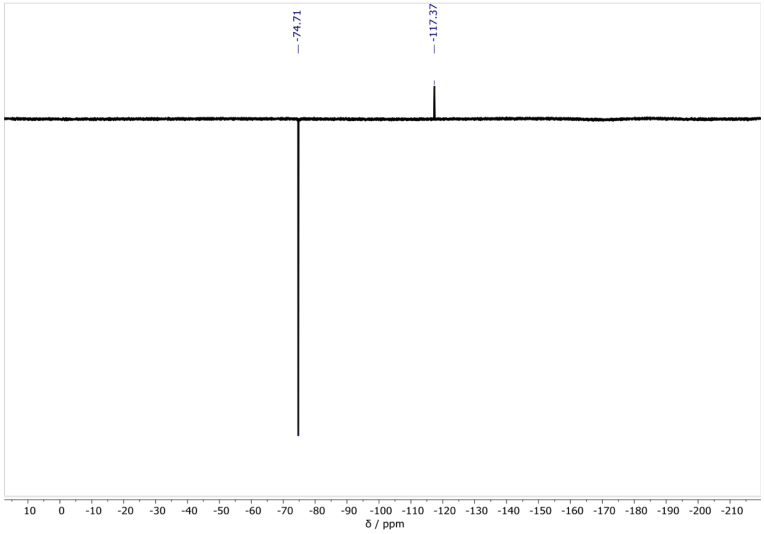

Figure S13. ^{19}F NMR of hydrazine-Cys-Sar-Cys-Sar-Cys-4-fluorobenzylamine (10) in DMSO-d_6.